Stable sound decoding despite modulated sound representation in the auditory cortex

Akihiro Funamizu[1,2*], Fred Marbach[1,3], and Anthony M Zador[1]

[1]Cold Spring Harbor Laboratory, Cold Spring Harbor, NY 11724, USA

[2]Present address: Institute for Quantitative Biosciences, the University of Tokyo, Tokyo, 1130032, Japan

[3]Present address: The Francis Crick Institute, NW1 4AT London, UK

*Correspondence: funamizu@iqb.u-tokyo.ac.jp

Summary

The activity of neurons in the auditory cortex is driven by both sounds and non-sensory context. To investigate the neuronal correlates of non-sensory context, we trained head-fixed mice to perform a two-alternative choice auditory task in which either reward or stimulus expectation (prior) was manipulated in blocks. Using two-photon calcium imaging to record populations of single neurons in auditory cortex, we found that both sensory and reward expectation modulated the activity of these neurons. Interestingly, the optimal decoder was stable even in the face of variable sensory representations. Neither the context nor the mouse's choice could be reliably decoded from the recorded auditory activity. Our findings suggest that in spite of modulation of auditory cortical activity by task priors, auditory cortex does not represent sufficient information about these priors to exploit them optimally and that decisions in this task require that rapidly changing sensory information be combined with more slowly varying task information extracted and represented in brain regions other than auditory cortex.

Introduction

Appropriate choices based on sensory stimuli are critical to survival. An animal hears a sound, such as a mouse's squeak or an owl's hoot, and must decide whether and how to respond to it. The appropriate response depends not only on what the stimulus is, but also on the behavioral context. This behavioral context includes the animal's present and previous experience, including its memories about what sounds it has heard recently and what previous choices were successful. Thus, an animal's response to sensory stimuli adapts to behavioral context.

Contextual adaptation of neural responses occurs throughout the auditory system, from the cochlea to the auditory cortex and beyond. These adaptations allow for better use of limited resources, such as dynamic range (in the case of feedback to the cochlea) or limited attentional resources (Hubel et al. 1959). Sound responses in auditory cortex and elsewhere in the auditory stream are also modulated by many task variables, including sound statistics (Ulanovsky et al. 2003), task engagement (Otazu et al. 2009), movement (Schneider et al. 2014), spectral attention (Fritz et al. 2003), and fear (Quirk et al. 1997). Contextual modulation of sound-evoked responses represents a ubiquitous feature of auditory, as well as non-auditory, sensory representations.

To drive behavior, neural representations formed in the auditory cortex must be "decoded" (Bialek et al. 1991; Ma et al. 2006) by the downstream areas to which it projects. Here we address two questions about the decoding of auditory cortical representations. First, we ask whether noise in the cortical representation of auditory stimuli constrained the performance of animals performing an auditory discrimination task. Second, we ask how downstream brain areas can decode neural representations in the auditory cortex if those representations are themselves changing because of contextual adaptation. Intuitively, one might imagine that changing representations might lead to miscommunication between brain areas, for the same reason that changing the meaning of red and green at traffic lights might disrupt traffic flow.

To address these questions quantitatively, we have developed a two-alternative choice (2-AC) auditory decision-making task in which we could manipulate either of two contextual variables: stimulus probability or reward size (The International Brain Laboratory et al. 2021; The International Brain Laboratory 2017; Platt and Glimcher 1999; Hanks et al. 2011; Feng et al. 2009). To maximize reward in this task, subjects must combine stimulus information with the context: stimulus + context → choice. Using two-photon (2P) calcium imaging to record the simultaneous activity of hundreds of neurons in the auditory cortex while mice were performing either the stimulus-probability or reward-size task, we examined what could be decoded from auditory cortical activity in the face of adapting representations.

Here we report that although changes in both reward and stimulus contexts modulated neural representations of sound in the auditory cortex, the optimal decoder for sound was remarkably invariant to different encodings. In many behavioral sessions, decoding the activity of one or a small handful of neurons matched or exceeded the performance of the animal on a trial-by-trial basis, suggesting that cortical noise did not limit the animals' performance during this task. By contrast, neither context nor choice could be reliably decoded from auditory cortical activity as behavioral context varied, implying that the animals' decisions depended on the integration of information represented outside of auditory cortex. Our results demonstrate that sound stimuli are encoded by the auditory cortex, and can be reliably and stably read out by downstream areas, even when the encoding is modulated by behavioral context. The stability of auditory cortical

sound decoding suggests that plasticity in brain areas downstream of the auditory cortex likely mediate behavioral adaptation induced by changes in behavioral context.

Results

We first show that mice exploit changes in behavioral context (reward size or stimulus probability) to optimize choices in a 2-AC auditory decision task. Then, using two-photon calcium imaging of neuronal activity in primary auditory cortex, we establish that sound-evoked neuronal responses are modulated by changes in behavioral context. Next, we construct decoders of neuronal activity, and show that decoding the activity of a small number of neurons—sometimes even a single neuron—matched or exceeded the performance of the animal. Finally, we show that sound decoding is stable, suggesting that (i) downstream areas of auditory cortex do not require context-dependent change of decoding weights to optimize the sound readout and (ii) plasticity in downstream areas is essential for context-based reward maximization.

Mice combine sensory stimulus and context in a perceptual decision-making task.

We developed a tone-frequency discrimination task for head-fixed mice (**Figure 1A and B**) (Marbach and Zador 2016). Mice were placed on a cylindrical treadmill facing three lick spouts. To initiate a trial, mice were required to lick the center spout, which triggered the delivery of a "tone cloud" sound stimulus composed of 58 overlapping brief pure tones (each pure tone 0.03 s, total 0.6 s). To motivate animals to withhold their choice, a 0.5 μl water reward was delivered at the center spout at the end of the stimulus, at which point the subject was required to lick the left or right spout depending on whether there were more low (5 – 10 kHz) or high (20 – 40 kHz) frequency tones in the tone cloud stimulus. Correct choices were rewarded with a sucrose water reward (5%, 2 μl), while incorrect choices resulted in a noise burst (0.2 s). The tone clouds were presented at six levels of difficulty (proportion high tones 0, 0.25, 0.45, 0.55, 0.75, 1).

On alternating sessions, we manipulated either the stimulus probability (the fraction of trials where the stimulus was of the high or low category) or the reward amount. In the stimulus probability task, the stimulus probability for each category alternated between 70%-30% and 30%-70% in blocks of 200 trials (**Figure S1A**). Thus in a 70%-30% block, the stimulus was drawn with 70% probability from one of the three stimuli for which a left response was rewarded (0%, 25%, 45% high-frequency tones). In the reward amount task, the reward amount (3 μl or 1 μl) associated with correct left and right choices varied in blocks of 200 trials, holding the stimulus probability at 50%-50%.

In each case, the optimal behavior in the face of sensory uncertainty is to make biased decisions. Performance in the task varied smoothly with trial difficulty, with near perfect performance on easy trials (0 or 1 proportion high tones; example session and tone cloud in **Figure 1B and C**) and performance near chance on difficult trials (0.45 or 0.55 proportion high tones). The animal

could exploit the context to achieve a higher reward rate especially on the difficult trials. If the animal was in a 30%-70% block where high frequency (rightward) trials are more common than low frequency trials, the mouse should choose rightward more often. Similarly, if the animal was in a block of 1μl-3μl in the reward amount task on difficult trials, the best strategy is to choose rightward. The optimal strategy can be computed based on the task structure (context) and the estimated uncertainty about the stimulus.

We analyzed 83 pairs of stimulus probability and reward amount sessions (166 sessions in total). The choice behavior of mice was significantly biased to the side associated with the high stimulus probability or large reward amount (**Figure 1D**) ($p = 4.7E-15$ and 2.6E-15 in two-sided Wilcoxon signed rank test in the stimulus and reward tasks, 83 sessions in each task), confirming that as expected mice used the contextual information to modify their actions to increase their reward rate. The bias in behavior was consistent across mice (**Figure S1B**). A logistic regression analysis revealed that the stimulus probability and reward amount affected the choices but did not affect the stimulus sensitivity (slope of psychometric curve) or lapse rate (error rate at 0 % and 100 % high tones) (**Figure 1E**).

We also used the behavioral data to assess whether the mice made optimal use of the context. To compute the optimal strategy, we assumed an ideal observer with a stimulus sensitivity estimated from the mouse's psychometric curve (Green and Swets 1966; Britten et al. 1992; Pisupati et al. 2021). We found that the subjects' behavior on the stimulus probability task was considerably less biased than that predicted from an ideal observer model (two-sided Wilcoxon signed rank test, $p = 1.0E-14$) (**Figure 1F**), but only slightly suboptimal for the reward task ($p = 0.017$). These are consistent with the observation that the ideal observer obtained more reward than the mice (two-sided Wilcoxon signed rank test, $p = 2.3E-12$ and 3.0E-9 in the stimulus and reward tasks, each 83 sessions), although mice obtained more reward than an unbiased behavior model with same stimulus sensitivity ($p = 0.0087$ and 5.7E-11). The difference in the observed behavioral bias between the stimulus and reward tasks may arise in part from the fact that subjects can detect a block switch on a single trial for the reward task (because the reward amount on a given port changes by a factor of three), whereas detecting changes in stimulus probability between blocks requires multiple trials. Thus the behavioral data indicate that the mice are exploiting information about context to increase their reward rate.

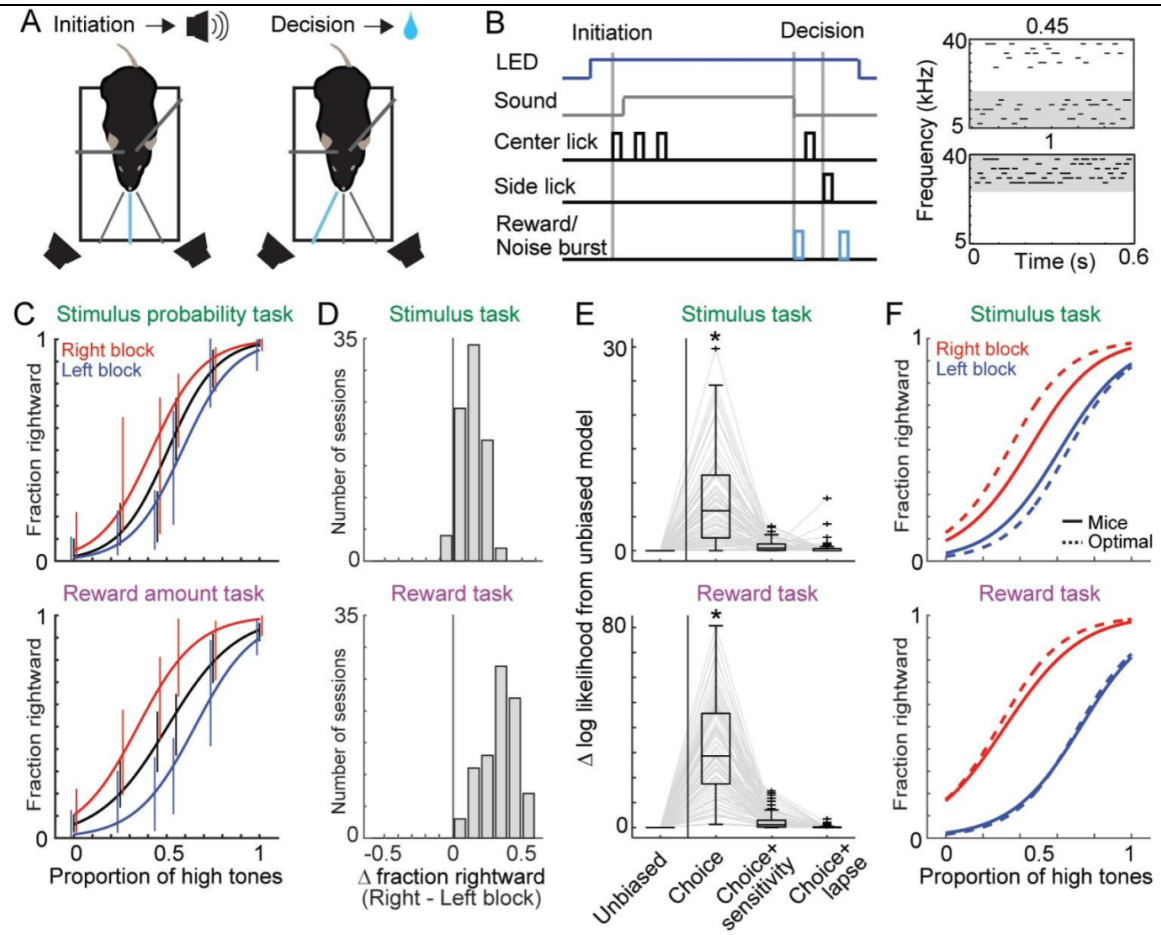

Figure 1. Stimulus probability and reward amount bias choice in auditory discrimination task (**A**) Setup. (**B**) Trial structure. A blue LED indicated the end of the inter-trial interval. Trials were self-initiated: licking the center spout triggered the sound stimulus (0.6 s), at the end of which 0.5 µl of water was delivered on the center spout. Any side-lick thereafter triggered a sucrose reward (correct) or a noise burst (error). Two example stimuli (tone clouds) are shown with a proportion of high frequency tones 45 % (*top*) and 100 % (*bottom*). Black lines denote 30 ms pure tones. (**C**) Choice behavior in one session. Error bars show 95 % confidence intervals. The choices were fit with a logistic regression ('Choice' in (**E**)). (**D**) Choice bias in all the 83 sessions. Change in fraction rightward shows the difference of average choice probability in the logistic regression between the left and right blocks (6 mice in each task). (**E**) Choice selective bias. Logistic regression tested whether the choices during the task had no bias depending on blocks (Unbiased), only bias in the choices (Choice), bias in the choices and sound sensitivity (Choice + sensitivity), or bias in the choices with non-zero lapse rate (Choice + lapse). Change in log likelihood in 'Choice' showed the increase of log likelihood from 'Unbiased'. Change in log likelihood in 'Choice + Sensitivity' and 'Choice + Lapse' showed the increase of log likelihood from 'Choice' (83 sessions; central mark in box: median, edge of box: 25th and 75th percentiles, whiskers: most extreme data points not considered outliers (beyond 1.5 times the inter-quartile range), here and hereafter; * $p < 0.001$ in likelihood ratio test in averaged log likelihood per session). (**F**) Suboptimal choice behavior. Bold lines show the mean psychometric functions in 83 sessions. Dotted lines show the optimal behavior estimated from the stimulus sensitivity in 'Choice' model.

Two-photon microscopy in the auditory cortex during two tasks.

We imaged calcium activity from six mice expressing GCaMP6f in excitatory neurons (see Methods). All the mice performed both tasks. Because the auditory cortex is located on the side of the head, the objective lens for imaging was placed diagonally, allowing the mouse to remain in a more comfortable configuration parallel to the ground (**Figure 2A**). We first identified the location of primary auditory cortex using one-photon wide field imaging (**Figure 2B**). A 4-kHz pure-tone evoked a characteristic constellation of activity in primary, anterior and secondary auditory fields (A1, AAF and A2 (or SRAF)) (Issa et al. 2014; Romero et al. 2020). The most posterior activity spot was identified as A1, which was target of further detailed study using two photon microscopy.

In each field of view (FOV), we investigated the frequency tuning of neurons by presenting pure tones with various frequencies (**Figure 2C**) to passive animals. We imaged three xy planes at varying depths along the z-axis to sample layers 2 and 3. On average, 13% (36 / 280) of neurons per FOV showed tone-evoked activity in at least one frequency ($p < 0.005$ in one-sided Wilcoxon signed rank test); the relatively low fraction of tone-responsive neurons is consistent with previous reports in various preparations (Hromádka et al. 2008; Jaramillo et al. 2014; Runyan et al. 2017). We defined a neuron's best frequency (BF) as the frequency which elicited the highest activity. The BF map, constructed as the average of neurons over the z axis, showed tonotopy in imaged regions (example mouse, **Figure 2D**; all mice, **Figure S2**).

To image the activity of the same neurons during both the stimulus probability and reward amount tasks, we switched the task on alternate days, keeping the same FOV (**Figure 2E**). We used a software package, Suite2P (Pachitariu et al. 2007), to detect overlapping regions of interest (ROIs) between the tasks, as well as to detect ROIs from raw imaging data. In total, Suite2P detected 23088 and 23350 ROIs in the stimulus probability and reward amount tasks, respectively (278 and 281 ROIs on average per FOV). Suite2P extracted 17523 overlapping ROIs (211 ROIs per FOV).

We identified task-relevant neurons from the overlapping ROI (**Figure 2F**). We defined a "task-relevant neuron" as any neuron showing increased activity in at least one of the following 6 time windows compared to the inter-trial interval in either the stimulus probability or reward amount task: (i) before the sound onset; (ii) during the sound presentation; (iii) between 0 and 1 sec from the choice; (iv) between 1 and 2 sec from the choice; (v) between 0 and 1 sec from the reward or noise-burst delivery; (vi) between 1 and 2 sec from the reward or noise-burst delivery. In each time window, the neural activity was analyzed in 3 different trial types depending on the sound category or choice. There were 2 task settings, 6 time windows, and 3 trial types (36 settings in total (6 x 3 x 2)). We identified 13581 task-relevant neurons out of 17523 overlapping neurons (78 % of ROIs per FOV on average, one-sided Wilcoxon signed rank test $p < 0.001$ in each comparison). The peak activity time and signal strength of task-relevant neurons were correlated across days (Spearman correlation, time: $r = 0.56$, $p = 0$, strength: $r = 0.72$, $p = 0$) (**Figure 2G and S3**), consistent with a previous finding in mouse parietal cortex (Driscoll et al. 2017).

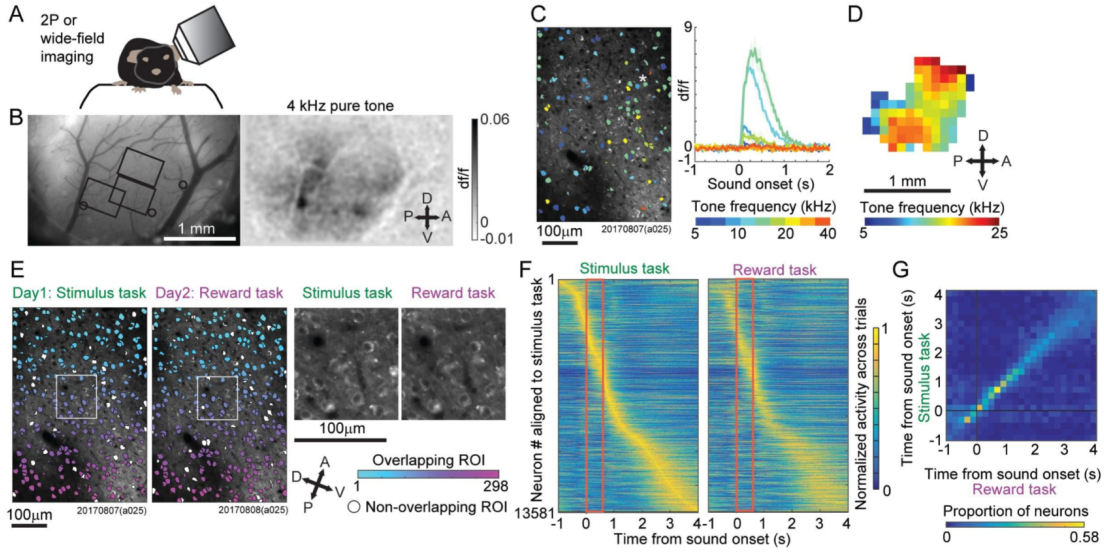

Figure 2. Two-photon microscopy in the auditory cortex during two tasks

(**A**) Setup for microscopy. Objective lens for microscope had a tilted angle to keep the mice parallel to the ground. (**B**) Identification of primary auditory cortex with one-photon wide-field imaging. The 4-kHz pure tone evoked responses through the cranial window provided the locations of the primary, anterior, and secondary auditory fields (*right panel*). Three circles in the left panel show the approximate peak location of the tone evoked responses. Three rectangles show the imaging locations of two-photon microscopy in the example mouse. The depth of imaging field was different in every session. (**C**) Tone evoked responses in one field of view in two-photon microscopy. The color of each region of interest (ROI) shows the best frequency (BF). ROIs with no color did not show significant sound evoked activity. Example calcium traces with means and standard errors are shown in the ROI with asterisk. (**D**) Tonotopy in the imaged location. The BF map of each field of view was merged and superimposed in z axis to show the BF map in xy plane. The BF of each xy location was analyzed as the average BFs of neurons. (**E**) Identification of overlapping ROIs imaged during both the stimulus and reward tasks. The colored and white ROIs were detected as overlapping and non-overlapping, respectively. The magnified view of square site is shown on the right. (**F**) Average activity of task-relevant neurons across trials. The activity was normalized between 0 and 1 and aligned based on the peak activity timings in the stimulus task. (**G**) Peak activity timings of neurons across tasks. Based on the peak timings in reward task (x axis), the proportion of peak timings in stimulus task is shown (y axis; the sum of each column is one) (n = 13581, task-relevant neurons).

Sound responses are modulated by the stimulus and reward context.

We next tested if the activity in auditory cortex was modulated by the block-wise changes in stimulus or reward context. Among the task-relevant neurons, we focused on sound-responsive neurons showing increased activity during stimulus presentation in the stimulus probability and reward amount tasks (one session in **Figure 3A,** 83 sessions in 2909 and 2573 neurons; 17% and 15% per FOV on average; Kruskal-Wallis test, $p < 0.01$). Of these, 1735 neurons (11% per FOV) increased activity during both tasks. The preferred tone cloud was preserved between the two tasks (**Figure 3B,** Spearman correlation, $r = 0.81$, $p = 0$), and correlated with the best frequency during passive pure tone presentation (**Figure S4**, $r = 0.32$, $p = 1.4E-14$ in stimulus task; $r = 0.36$, $p = 1.4E-17$ in reward task). The fraction of neurons responsive to sounds during the task was comparable to the fraction responsive to pure tones during passive listening (13%), but much smaller than the 78% of neurons that were modulated by the task. Thus, consistent with previous findings in auditory cortex (Jaramillo et al. 2014), most task-responsive neurons were not sound-responsive.

We investigated the contextual modulation of sound responses by comparing the activity between left and right blocks within each task. A representative sound-responsive neuron showing increased activity in the right block during the stimulus probability task is shown in **Figure 3C**. We then aligned the activity of each neuron based on its "preferred block," i.e. the block associated with the preferred tone cloud stimulus for that neuron. Specifically, the preferred block was "left" for neurons whose preferred tone cloud was low, whereas it was "right" for neurons whose preferred tone cloud was high. We compared activity between blocks elicited during the preferred tone cloud stimulus and found that the activity could be modulated in either the positive or negative direction (**Figure 3E**). Contextual modulation was stronger in the neurons tuned to the difficult and moderate tone clouds and weaker for those tuned to easy tone clouds (**Figure 3E and S5**), irrespective of choices (**Figure S6**). We then analyzed the median block modulations of sound responsive neurons in each session (**Figure 3F**). This population block modulation was larger in the reward task than in the stimulus task. These results indicate that the encoding of sound by neurons in auditory cortex is modulated by the stimulus or reward expectation and that the magnitude of the neuronal modulation is proportional to the behavioral bias.

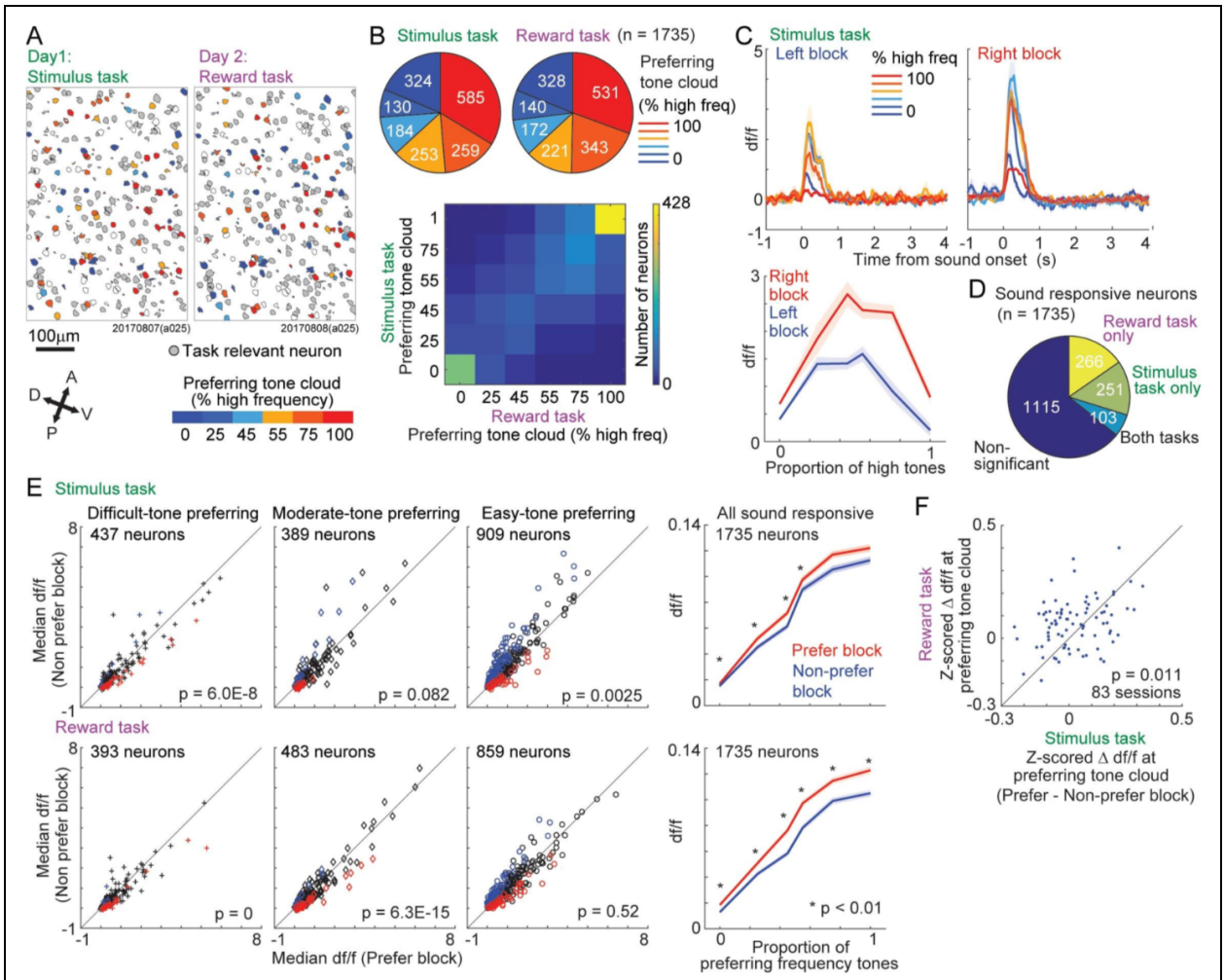

Figure 3. Sound responses are modulated by context about stimulus probability and reward amount

(**A**) Sound responsive neurons in an example field of view (FOV) in **Figure 2E**. The colored, gray and white neurons were sound responsive, task-relevant and overlapping neurons, respectively. (**B**) Preferring tone cloud of neurons that were sound responsive during both the stimulus and reward tasks (n = 1735). Scatter plot showed the preserved preferring tone cloud across tasks (Spearman correlation, r = 0.81, p = 0). (**C**) Traces of one neuron during left- and right-block trials in the stimulus probability task. (*Bottom*) Tuning curve shows the activity during sounds. Means and standard errors. (**D**) Number of sound responsive neurons with context modulation ($p < 0.05$, two-sided Mann Whitney U-test at preferring tone cloud). (**E**) Context modulation of sound responsive neurons. Sound responsive neurons were categorized to the difficult, moderate, and easy neurons depending on their preferred tone clouds. Scatter plot compared the activity of the preferred tone cloud between blocks. The red and blue points show the significant increase of activity in the preferred and non-preferred block, respectively ($p < 0.05$ in two-sided Mann-Whitney U test). P-value shows the population comparison with two-sided Wilcoxon signed rank test. The activity was aligned to the preferred tone category. Tuning curve shows the medians and robust standard errors of activity of sound responsive neurons in the preferred and non-preferred blocks (*, $p < 0.01$ in two-sided Wilcoxon signed rank test). (**F**) Comparison of block-modulated activity between the stimulus and reward tasks. In each session, we analyzed the median block modulation of sound responsive neurons (two-sided Wilcoxon signed rank test).

Neural decoding of stimulus category is comparable to mouse behavior.

We next asked how other brain areas could make use of neural representations in auditory cortex to decode the behaviorally relevant category (low- or high- frequency) from which a particular tone cloud stimulus was drawn. We first quantified the decoding performance of single neurons during sound presentation (0.6 s) over the whole session (ignoring the block structure), using a model in which downstream areas decode the stimulus category by setting an optimal threshold on the recorded Ca signal (**Figure 4A**). In general, single neurons performed remarkably well. Indeed, we found that, in a significant fraction of sessions (25% and 55%, respectively, out of 83 sessions in the stimulus and reward tasks), the performance of an ideal observer decoding the best single neuron was better than that of the mouse itself during that session (**Figure 4B, C and D**), consistent with similar observations in primates (Britten et al. 1992).

We then quantified the decoding performance of the entire neuronal population recorded simultaneously. We used a sparse logistic regression (SLR) decoder, with nested 10-fold cross validation (**Figure 4E**) (Shimizu et al. 2015). We chose the SLR decoder because it performed as well as or better than other decoders tested (**Figure S7A**), and because it has a natural interpretation as a readout by a population of downstream neurons. We again selected the weights optimal for decoding the stimulus category. The neurometric function obtained from this optimal SLR decoder was analyzed by binarizing the probabilistic estimates (**Figure 4F**). To avoid overfitting the SLR was fitted with an L1 regularizer which identified sparse subsets of neurons for decoding (**Figure 4G**).

As expected, decoding by the population was better than decoding by single neurons (**Figure S7B**), indicating that the representation of sound was distributed across the population. Population decoding was also often better than the performance of the animal, even when the biases were not exploited by the neural decoder (**Figure 4H)**. That is, the decoder was trained and tested using all trials, regardless of whether they were from a left or right block. All the decoding performance was tested using neuronal activity elicited during sound presentation (0.6 s). One possible concern is that this relatively long time window might in principle exceed the window over which mice accumulate sound evidence and thus might provide the optimal neural decoder with an unrealistic advantage compared with the mouse's behavior (**Figure S8**). However, behavioral analysis suggested that mice did indeed accumulate evidence over the entire sound presentation (**Figure 4I**), suggesting that the accumulation was not responsible for the superior performance of the neural decoder. Thus, the optimal readout of both single neurons and neural populations often matched or exceeded the mouse's performance on a given session.

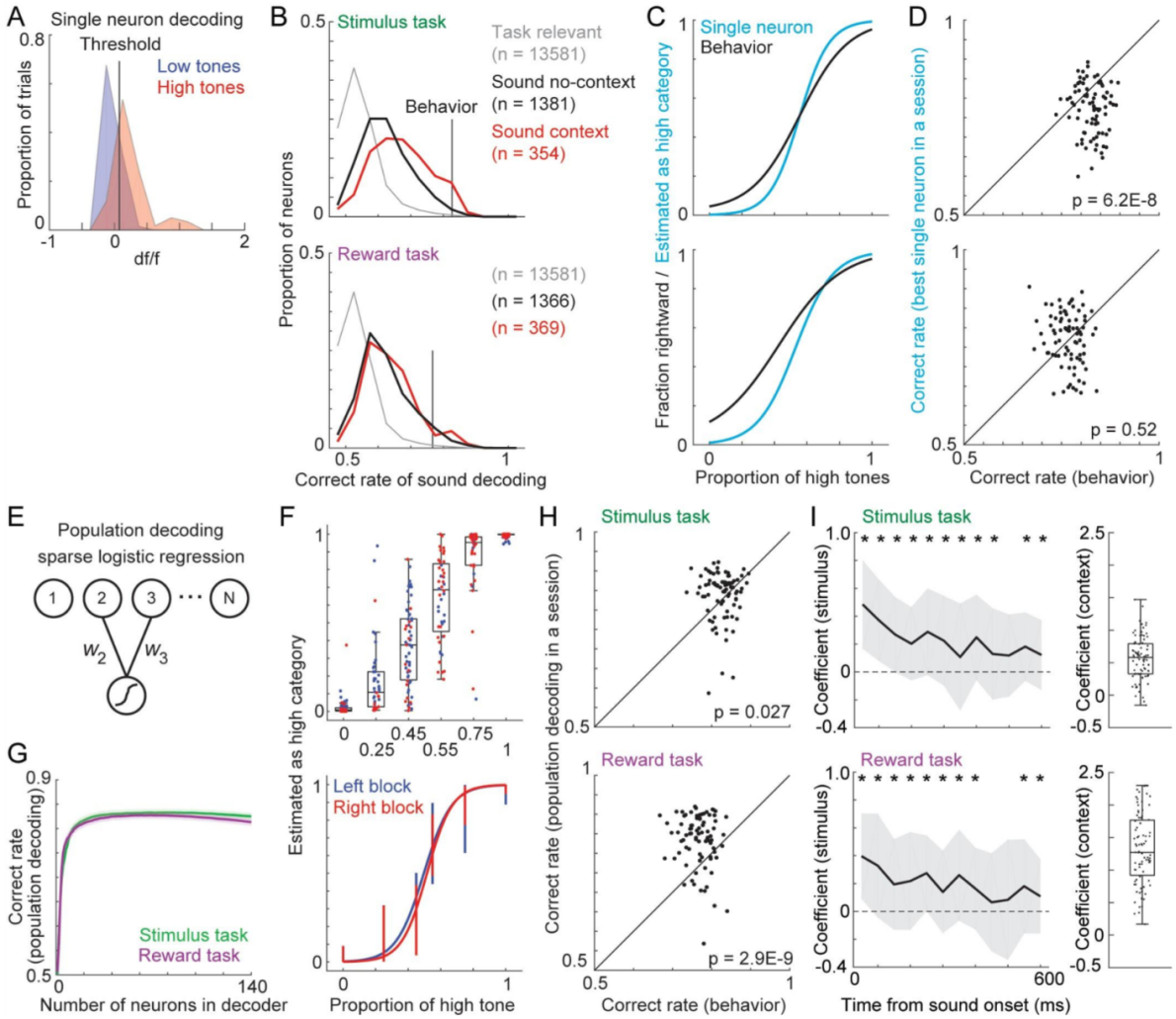

Figure 4. Comparable performance of neural sound decoding and mouse behavior

Sound decoding in single neurons. (**A**) We optimally identified a threshold to discriminate the high- and low-category tones in each neuron (cross validation). (**B**) Distribution of correct rate in single neurons. The vertical bar shows the average correct rate of mice behavior (83 sessions). Sound responsive neurons are separated into context modulated (*red*) and non-modulated (*black*). (**C**) Neurometric and psychometric functions in single session. The neurometric function was analyzed from the best sound-decoding neuron in a given session. (**D**) Scatter plot comparing the sound discrimination between the best single neuron and mouse behavior in each session. Single neurons often outperformed the mouse behavior (two-sided Wilcoxon signed rank test in 83 sessions). (**E**) Population sound decoding with sparse logistic regression (SLR). SLR sparsely extracted neurons for decoding. (**F**) Sound decoding in one session. Each point shows the estimated probability of high tone category in each trial (400 trials) (*top*). The probabilistic sound estimation was binarized at 0.5 to analyze the neurometic function. (*bottom*) Error bars show the 95 % confidence intervals. (**G**) Means and standard errors of correct rate of SLR as a function of number of neurons (83 sessions in each task) (**H**) Comparison of performance between neuronal population and mouse behavior (two-sided Wilcoxon signed rank test in 83 sessions). (**I**) Psychophysical kernels. Logistic regression analyzed how tones at each time point and the context information contributed to the choice behavior. Medians and median absolute deviations (*left*, * $p < 0.01$ in two-sided Wilcoxon signed rank test in 83 sessions).

Noise correlation among neurons with same tuning constrains sound decoding performance.

Although as expected population decoding was consistently better than single neuron decoding on single-trials (**Figure S7B**), in some cases the advantage gained from using extra neurons in the decoder was relatively small. If extra neurons each carried independent information about the stimulus, then we would expect the inclusion of additional neurons to improve the performance of the decoder; but if the information represented by different neurons is redundant, then the decoding performance will saturate. We therefore examined the role of single-trial correlations in limiting the readout of the sensory signal from the neuronal population (Averbeck et al. 2006; Miura et al. 2012; Moreno-Bote et al. 2014).

We first investigated the "signal correlations," defined as the correlation between the average stimulus-evoked calcium activity for each of the 6 tone clouds, for all sound-responsive neurons. As expected, signal correlations were higher among neurons with the same preferred tone cloud than neurons with different preferences (example session in **Figure 5A**; 83 sessions in **Figure 5B**, $p = 0$ in two-sided Mann Whitney U-test). We then explored noise correlations and found a similar tendency. The activity of neurons with similar stimulus-driven responses were more correlated on single trials than those with different responses (**Figure 5A and C**, $p = 0$ in two-sided Mann Whitney U-test). Noise correlations were higher between neurons with same preferred stimulus independent of the distance between them (two-sided Mann Whitney U-test $p = 0.049 - 0$, binned every 100 μm of distance between neurons), indicating the higher noise correlation was not simply a consequence of the tendency of similarly tuned neurons to be closer on the tonotopic map.

To assess the effect of these noise correlations on stimulus decoding, we compared the performance of a decoder acting on single-trial activity to the performance of a decoder with access to uncorrelated activity obtained on scrambled trials. As expected, decoding based on scrambled trials continued to improve as more neurons were included in the decoder, whereas the performance of the single trial decoder reached an asymptote after around 10-20 neurons and reached the 95 % of maximum correct rate with 8 neurons on median (**Figure 5D**). These results confirm the role of noise correlations in limiting the potential for reading out activity from a population of neurons. However, the fact that the performance of even the single-trial population decoder often outperformed that of the animal itself (**Figure 4**) suggests that these noise correlations were often not the sole or even main factor in limiting the animals' performance.

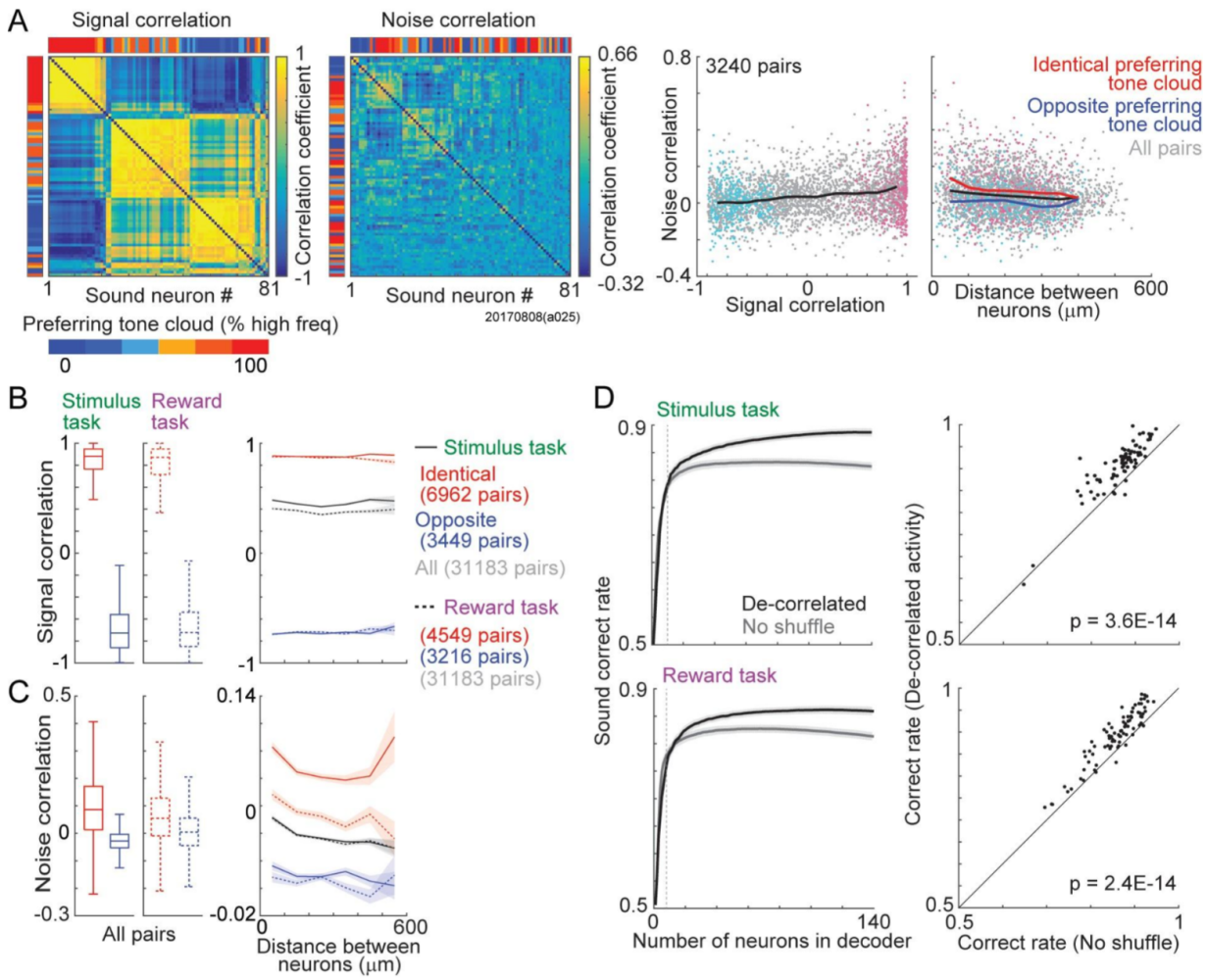

Figure 5. Noise correlations limit sound decoding

(**A**) Signal and noise correlations in one session. Cross correlogram shows the correlations between sound responsive neurons, sorted using hierarchical clustering. Color bars at the top and left show the preferring tone cloud of neurons. Scatter plot shows the relationships among signal correlations, noise correlations, and the physical distance between neurons. Red and blue dots show the data from neurons with same and different preferring tone cloud, respectively (easy stimuli only). Lines show the moving average. (**B**) Signal correlation in 83 sessions. (*Left*) Box plots compared the signal correlation between neuron pairs of same and different preferring tone clouds. (*Right*) Signal correlation in all neuron pairs as a function of distance between neurons. (**C**) Noise correlations, as in **B**. High noise correlations in the neuron pairs with same preferring tone cloud were observed irrespective of distances. (**D**) Noise correlations limit performance. Means and standard errors (*left*). Vertical dot line shows the median number of neurons achieved the 95% of maximum correct rate of population decoding. We extracted the neurons achieved the highest correct rate in non-shuffled activity and compared the correct rate with the de-correlated activity (*right*) (83 sessions, two-sided Wilcoxon signed rank test).

Optimal decoder for stimulus category is stable.

Our previous analyses indicate that cortical noise is not the sole or even main factor limiting the performance of the animal on this task, suggesting that the performance is limited by representations outside of auditory cortex. This raises the question: How can downstream brain areas decode neural representations in the auditory cortex, if those representations are themselves changing because of contextual adaptation? One might imagine that changing representations might lead to miscommunication between brain areas, for the same reason that changing the meaning of red and green at traffic lights might disrupt the flow of traffic.

To maximize reward in this task, an ideal observer (as a model of areas downstream of auditory cortex) with access to the neural activity in the auditory cortex, and with perfect knowledge of context, would make choices by combining auditory activity and stimulus context as follows:

$$Optimal_choice = \boldsymbol{F}\,[\,Cortical_sound_representation(\text{stimulus, context}), \text{context}\,].$$

In this equation, the optimal choice is some function $\boldsymbol{F}$ of both the population response and the context. Context enters into the formation of optimal choice in two ways. First, it enters implicitly, by changing the neural representation of the sound itself, via the term "*Cortical_sound_representation*" (**Figure 3**). Second, context enters explicitly, by changing the optimal action for a given best estimate of sound category. For example, if the neural response encoding the auditory stimulus is completely ambiguous, then a context in which the higher reward is at the left port would dictate that the optimal choice would be "left". Thus, the optimal choice can be formed by first estimating the stimulus category from the neural response (given the context), and then selecting the choice that maximizes the reward (given the estimate of the stimulus category). Below we consider these two potential effects of context separately.

We first consider the *implicit* effect of context, through its action on the neural encoding of the stimulus. In principle, the optimal strategy for decoding the stimulus category from the context-modulated neural response would be to use different decoders for each of the two contexts. To quantify the effect of context on decoding, we therefore compared the performance of a "dynamic weights" decoding strategy to that of an invariant "constant weights" decoder (**Figure 6A**). When an invariant "constant weights" decoder (trained on data from both blocks) was used, performance was similar across blocks (**Figure 6B**; two-sided Wilcoxon signed-rank test, $p = 0.24$ and 0.036 in the stimulus and reward tasks). Moreover, sound decoding did not improve with a "dynamic weights" decoder in which weights were trained and tested with data within a block (**Figure 6C**; in this as in all analyses, performance was tested on out-of-sample trials, i.e. samples not used for training). Even using different blocks for training and testing (e.g. trained with trials from the left block, and tested with trials from the right block) led to only a modest decline in performance compared with the dynamic weights decoder (**Figure 6D**; 1.6 % and 0.37 % on median in the stimulus and reward tasks; $p = 1.1E\text{-}8$ and 0.0063 in two-way Wilcoxon signed rank test). Furthermore, the stimulus category was identified more accurately than the correct choice (**Figure S9A**). These analyses indicate that, in spite of changes in sound-evoked responses induced by manipulating context, the identity of the sound can be read out effectively by an invariant decoder that does not adapt to these manipulations.

We next consider the *explicit* effect of context on choice. We first compared the performance of a decoder which can exploit perfect knowledge of context ("non-autonomous choice model") with

one that does not exploit context ("no-context model") (**Figure 6E and 6F**). This comparison revealed the large impact that context can have in this task. The non-autonomous choice model achieved a larger amount of reward compared to the no-context model in 74 and 78 out of 83 sessions in the stimulus and reward task (**Figure 6F** *right*). However, since making an optimal choice in this task requires perfect knowledge of the context, we next attempted to determine the context using only information available from auditory cortex ("autonomous choice model"). Using the SLR decoder, we found that the context could only be imperfectly decoded from the population activity (**Figure 6G,** 66 % and 70 % on average, chance level 50%), and was insufficient to bias the neurometric function across blocks compared to the subjects' observed behavior (**Figure S9B**). In other words, it does not appear that the auditory cortex represents the behavioral context well enough to account for the observed context-dependent shifts in the psychometric curves. Taken together with the invariance of sound decoding, these analyses suggest that the mouse makes choices by combining the auditory stimulus with a representation about context which is encoded downstream (or outside) of the auditory cortex. We compared the shifts in the psychometric curve predicted by the non-autonomous choice model and no-context model to the observed behavior of the mice (**Figure 6H**). For both the stimulus and reward tasks, the observed behavior was intermediate between the two models. This suggests that, consistent with **Figure 1E**, the animal makes suboptimal use of the block structure of the task, but exploits more of the available context information than is easily decoded from activity in auditory cortex.

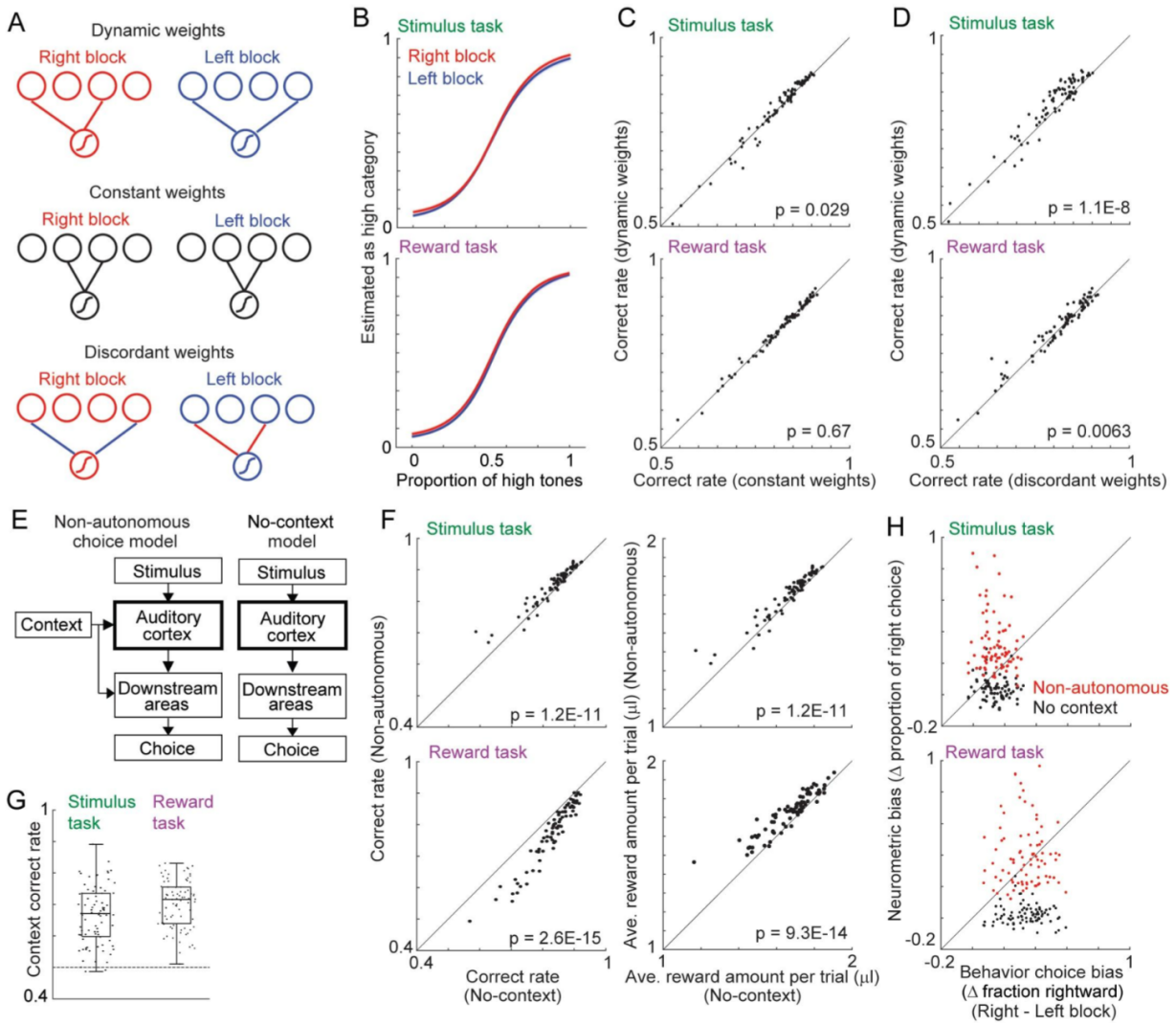

Figure 6. Stable sound readout from the auditory cortex

(**A**) Scheme of sound decoders. Decoder with dynamic weights trained and tested in the same block (optimal decoder). Constant weights had one series of weights across blocks. Discordant weights trained and tested with different blocks (e.g., trained the decoder in left block and tested in right block). (**B**) Means and standard errors of neuromeric functions in constant decoder (83 sessions in each task). (**C, D**) Comparison of decoding performance (83 sessions). Sound decoding with constant weights had comparable performance with the dynamic weights (two-sided Wilcoxon signed rank test). (**E**) Two models for how the mouse exploits context for choice. The non-autonomous choice model and no-context model assumed the perfect and no knowledge of context, respectively. (**F**) Comparison of decoding performance in correct rate of sound category (*left*) and received reward amount (*right*) (83 sessions, two-sided Wilcoxon signed rank test) (**G**) Context decoding from the auditory cortex (83 sessions). (**H**) Biases in the neuromeric functions across blocks compared with those in the mice behaviors. The bias was the difference of average right choice probability in neuromeric functions between blocks (two-sided Wilcoxon signed rank test: non-autonomous model, p = 1.0E-10 and 0.13 in the stimulus and reward tasks; no-context model, p = 5.3E-10 and 2.6E-15).

Shifts of decoding threshold are small compared to the contextual modulation of neurons.

The stability of the stimulus *decoder*, given the variability of the neural *encoding* of the stimulus, seems to pose a conundrum since we might expect that the optimal decoder would vary as the sound representation was modulated by changes in context. One straightforward resolution of this conundrum would be if the decoder relied only on neurons whose activity was not modulated by context. However, although as expected sound decoding relied mainly on sound-responsive neurons (**Figure S10**), the decoder relied on both neurons modulated by context and those not modulated by context (**Figure 7A**). This indicates that stable sound decoding was not achieved by relying only on neurons not modulated by context.

To resolve this apparent conundrum, we investigated the relationship between sound encoding and decoding in single neurons. **Figure 7B** shows a representative neuron with strong stimulus contextual modulation. However, even though contextual modulation was strong (**Figure 7B** *right*), the decoding threshold (*vertical green line, df/f*) was almost unchanged, suggesting that the change in decoding thresholds was small compared to the contextual modulation. This relationship was observed across the population of sound-responsive neurons **(Figure 7C** *left*), although the contextual modulations and changes in decoding thresholds were weakly correlated (Spearman correlation, $r = 0.13$ and 0.10 in the stimulus and reward tasks). The contextual modulations did not improve the decoding performance with dynamic weights (**Figure 7C** *right*) ($p = 0.65$ and 0.51). In these analyses, the decoding performance was estimated without cross validation to verify that the decoding with block-dependent weights was always better than a constant weight. These results indicate that the decoding filter of each neuron was relatively stable compared to the contextual modulation of neurons. One possible role of the contextual modulation was to improve the decoding performance (Spearman correlation, $p = 0$ and 2.8E-29 in the stimulus and reward tasks) (**Figure 7D**).

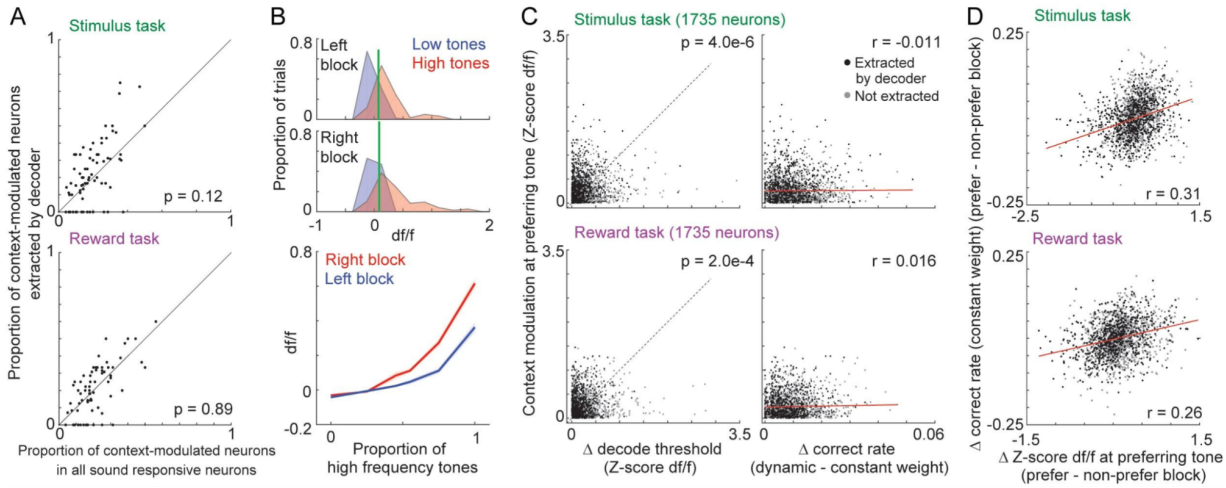

Figure 7. Context modulation of sound responses does not disrupt stable sound decoding
(**A**) Proportion of context-modulated sound responsive neurons extracted in sparse logistic regression (SLR) compared with that in all sound responsive neurons (two-sided Wilcoxon signed rank test, 83 sessions in each task). (**B**) Representative neuron with context-modulated activity and stable decoding filter. (*top*) Decoding thresholds (green lines) which separated the distribution of activity during low and high tones were similar between blocks. (*bottom*) Contextual modulation of activity. Data presentation same as in Figure 3C. (**C**) Decoding threshold, contextual modulation, and correct rate of sound responsive neurons. The contextual modulations were larger than the change in decoding threshold between blocks (*left*) (two-sided Wilcoxon signed rank test). Correlation between the decoding performance and contextual modulation (*right*). Contextual modulation was the absolute difference of neural activity at preferring tone cloud between blocks. (**D**) Contextual modulation improved decoding performance. Δ correct rate and Δ Z-score df/f show the difference of correct rate and the difference of activity between prefer and non-prefer block, respectively (Spearman correlation).

Choice readout from the auditory cortex.

Finally, we investigated whether the readout from the auditory cortex was only sound throughout the trial by analyzing the time course of sound and choice decoding with SLR (**Figure S11**). Here, to prevent the cross-talk between sound and choice decoding, sound decoding was analyzed within the trials of either the left or right choice (2 cases). The choice decoding was analyzed within the trials of the same tone cloud (6 cases). The performance of sound decoding became maximum around the sound offset, while the performance of choice decoding ramped up during sound and became maximum after the reward or noise burst delivery. The neural activity of sound-responsive neurons was modulated by choice even during the sound presentation (**Figure S12**), supporting the choice readout from the auditory cortex. Mice licked the side spouts already during sound on some trials (**Figure S6D**), but similar choice decoding was observed in trials without early side licks (**Figure S11C**).

Discussion

We have used two-photon calcium imaging to record the simultaneous activity of hundreds of neurons in auditory cortex in mice performing a context-dependent two-alternative choice auditory decision task. We find that (1) neuronal activity is context-dependent; (2) the activity of single neurons in auditory cortex in this task can often be decoded to yield performance as good or even better than the animal, and adding additional neurons often leads only to relatively minor improvements in performance; (3) the optimal decoder remains largely invariant, in spite of context-dependent changes in encoding. Our results suggest a model in which downstream areas can easily read out information about the stimulus from the activity in auditory cortex, in spite of context-dependent changes in activity.

Since the earliest recordings in auditory cortex, it has been clear that neuronal activity in auditory cortex is strongly modulated by non-sensory features. Hubel described neurons that "appear to be sensitive to auditory stimuli only if the cat 'pays attention' to the sound source" (Hubel et al. 1959). Subsequent studies revealed that neural responses are modulated by sound statistics, attention, task engagement and reward expectation (Fritz et al. 2003; Guo et al. 2019; Hubel et al. 1959; Otazu et al. 2009; Quirk et al. 1997; Schneider et al. 2014; Ulanovsky et al. 2003). Reinforcing the importance of such contextual modulation, we found that only 13% of neurons responded to tones presented during passive listening, whereas 78% of neurons responded to some component of the task, and about a third (36%) of sound-modulated neurons were modulated by changes in either reward amount or stimulus probability. This modulation raised questions about how downstream brain areas could reliably decode stimulus identity, in the same way that changing the red/green code for traffic lights might lead to traffic disruption.

To address these issues, we adopted a decoding approach (Bialek et al. 1996), and assessed how well an ideal observer, with access to activity of hundreds of auditory cortex neurons, could perform on this auditory decision task. In pioneering experiments, Newsome and colleagues (Zohary et al. 1994) related the activity of pairs of neurons in monkey area MT to decisions about motion direction. We found, in agreement with these early results, that single neurons could be decoded to yield performance comparable to that of the animal. This raised the question of why decoding the activity of multiple neurons simultaneously would not do even better. Newsome and colleagues, extrapolating from pairs of neurons, concluded that correlations among neurons limited decoding fidelity. In principle, such correlations could increase or decrease decodability of a population, depending on the nature of the correlations (Abbott and Dayan 1999; Moreno-Bote et al. 2014). Recent recordings of large neuronal populations with two-photon imaging have extended these results beyond pairs of neurons in the context of stimulus encoding (Rumyantsev et al. 2020). Here we have confirmed that the the same principles apply in auditory cortex: We have shown directly, in behaving animals, that decoding the activity of hundreds of auditory neurons simultaneously does not dramatically increase the neurometric performance compared with decoding the activity of just the few best neurons (**Figure 5D**).

Given the substantial fraction of neurons modulated by context in this task, we expected that the optimal decoding filter would vary in order to adapt to this modulation. Surprisingly, however, we found that a single linear decoder performed as well as one that adapted from block to block; the representation of stimulus was orthogonal to the representation of context (Knutsen and Ahissar 2009). In neural terms, this implies that there is no need for hypothetical downstream brain areas decoding the stimulus using the output of auditory cortex to "know" the behavioral context. On the other hand, at the behavioral level mice do exploit behavioral context in this task to maximize reward (**Figure 1**). This implies that the behavioral context is combined with stimulus information outside of auditory cortex (**Figure 6**). Candidate brain areas are the medial prefrontal cortex (Lak et al. 2020), parietal cortex (Hanks et al. 2011), retrosplenial cortex (Hattori et al. 2019), and anterior striatum (Kravitz et al. 2012). Neurons in these areas modulate the choice representations by stimulus or reward expectation. Note that we cannot be sure that the animal uses the representations in auditory cortex; demonstrating that would require a causal intervention, using either a transient or permanent lesion. However, the decodability of the representation in the face of modulation was nonetheless suggestive.

Supplemental figures

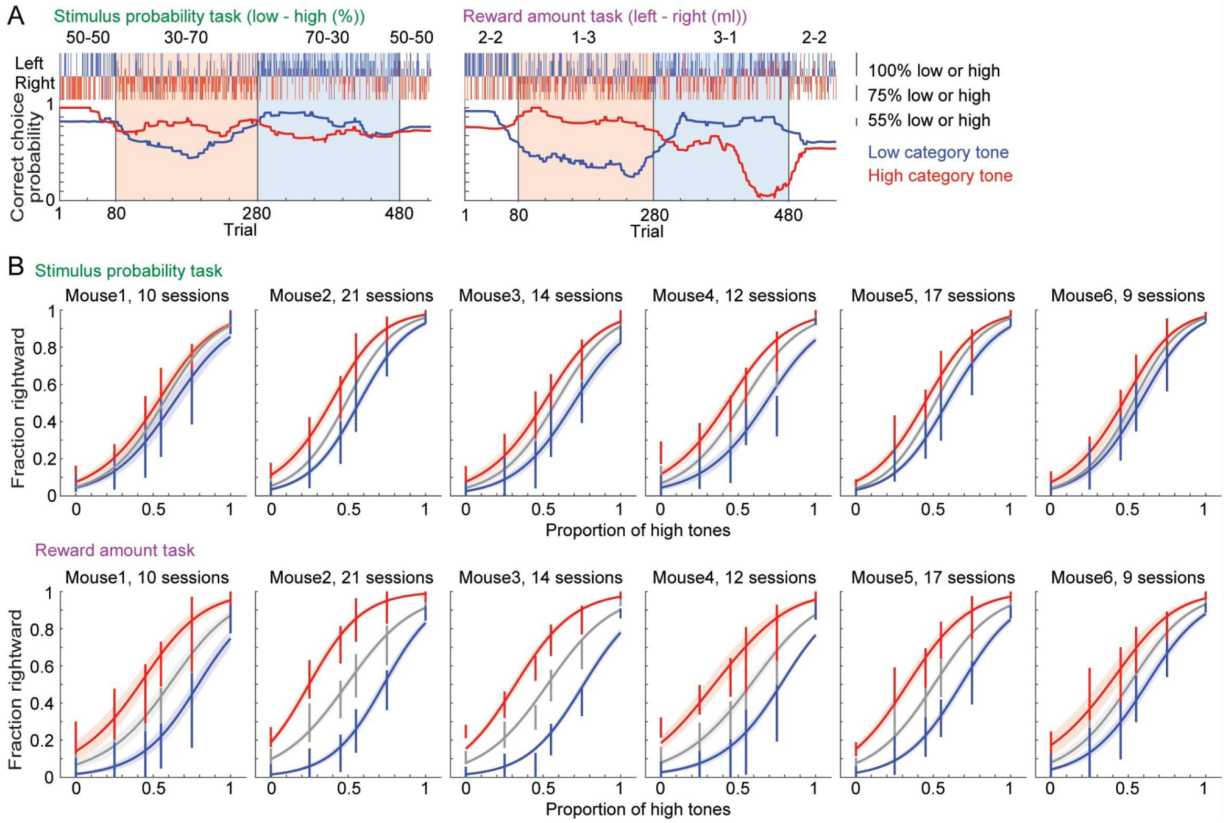

Supplemental Figure 1. Choice behavior in each mouse

(**A**) Block structure and choice behavior in example session. Top panels show the choice, tone category, and tone difficulty in each trial. Bottom panels show the moving averaged correct choice probability for low and high category tones. (**B**) Means and standard errors of psychometric functions are shown in each mouse. Logistic regression analyzed the psychometric function in each session ('Choice' in **Figure 1E**). Error bars show the standard deviations of choice probability per session.

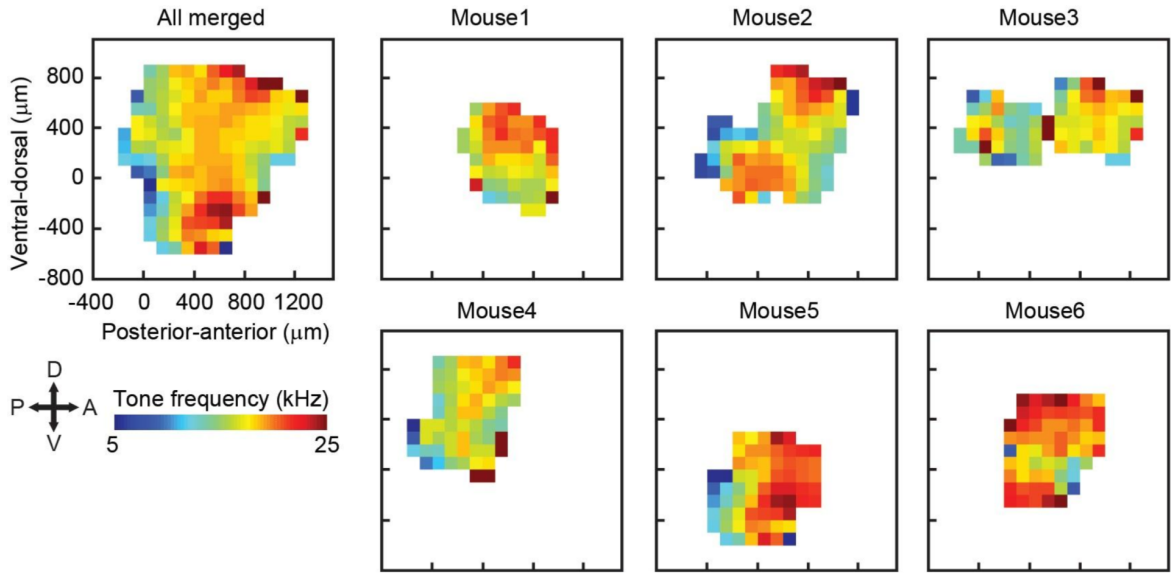

Supplemental Figure 2. Tonotopic map in each mouse

In each mouse, the best frequencies of pure-tone responsive neurons were superimposed in depth to make the tonotopic map in XY plane. Based on the 4-kHz tone evoked activity spot in the primary auditory cortex, the tonotopic map of each mouse was superimposed to make the merged map. This merged map was not used in the further analyses, as the tonotopic maps across mice were not precisely aligned in the coordinates.

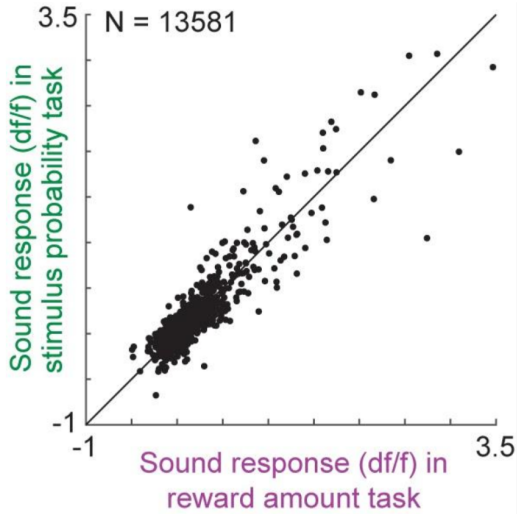

Supplemental Figure 3. Fluctuation of signal strength of neurons between stimulus probability and reward amount tasks

Median signal strength of single neuron during sounds (0.6 s) in all trials was compared between the tasks (Spearman correlation, r = 0.72, p = 0).

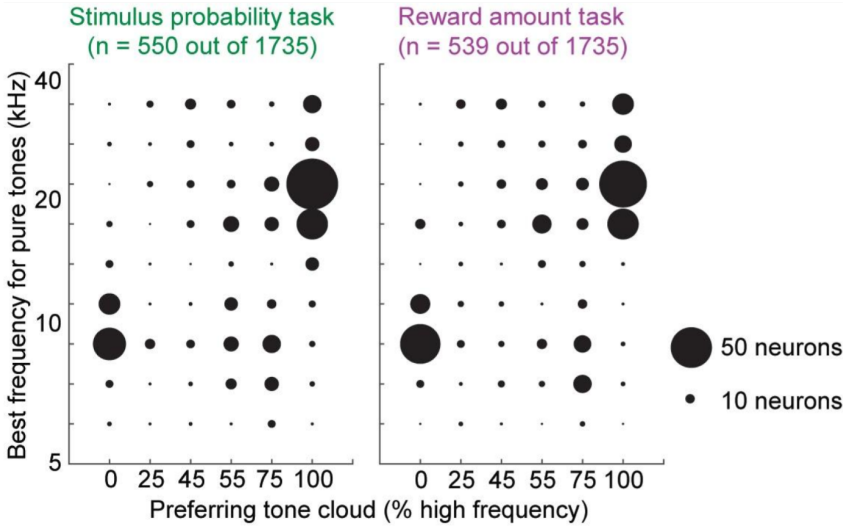

Supplemental Figure 4. Pure-tone best frequency of sound responsive neurons
In the stimulus probability and reward amount tasks, 550 and 539 out of 1735 sound responsive neurons showed the significant sound responses during passive listening outside the task. The pure-tone best frequency (BF) was defined as the frequency with the largest activity. When the neurons preferred the 100 % high- or low-frequency tone cloud, they tended to have the high or low BFs, respectively.

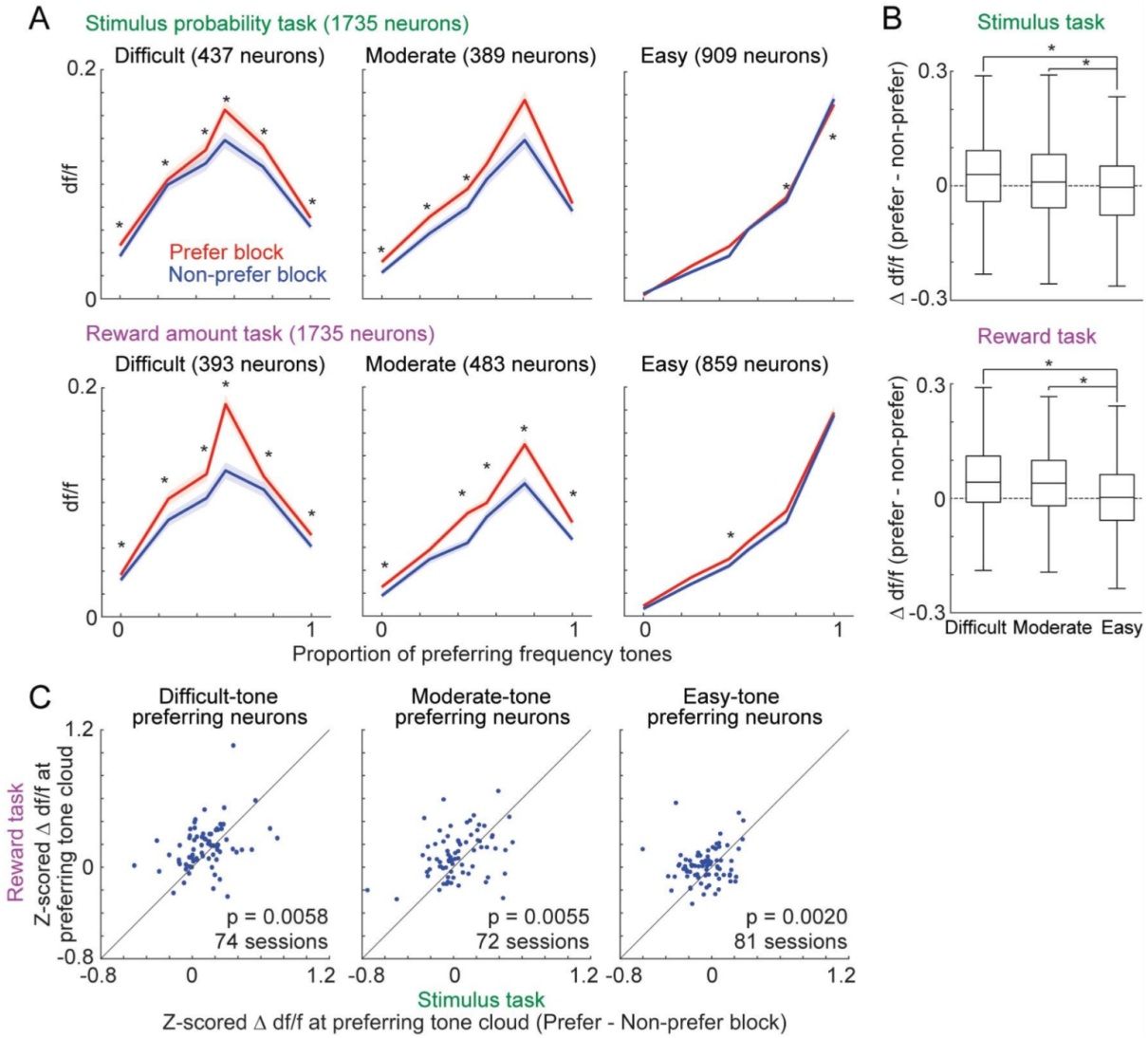

Supplemental Figure 5. Contextual modulation depends on preferring tone cloud of neurons
(**A**) Contextual modulation of sound responsive neurons in different preferring tone clouds. Sound responsive neurons were categorized to the (i) difficult, (ii) moderate and (iii) easy neurons depending on the preferring tone clouds in (i) 45 or 55 % high tones, (ii) 25 or 75 %, and (iii) 0 or 100 %, respectively. Medians and robust standard errors of population activity (*, $p < 0.01$ in two-sided Wilcoxon signed rank test). (**B**) Comparison of contextual modulation. Difficult and moderate neurons showed larger modulation than easy neurons (central mark in box: median, edge of box: 25th and 75th percentiles, whiskers: most extreme data points not considered outliers (beyond 1.5 times the inter-quartile range), here and hereafter. Plots without the outliers) (*, $p < 0.01$ in two-sided Mann Whitney U-test). (**C**) Comparison of median block-modulated activity per session between the stimulus and reward tasks. Data presentations comply with **Figure 3F** except that neurons were categorized to the preferring tone clouds (two-sided Wilcoxon signed rank test).

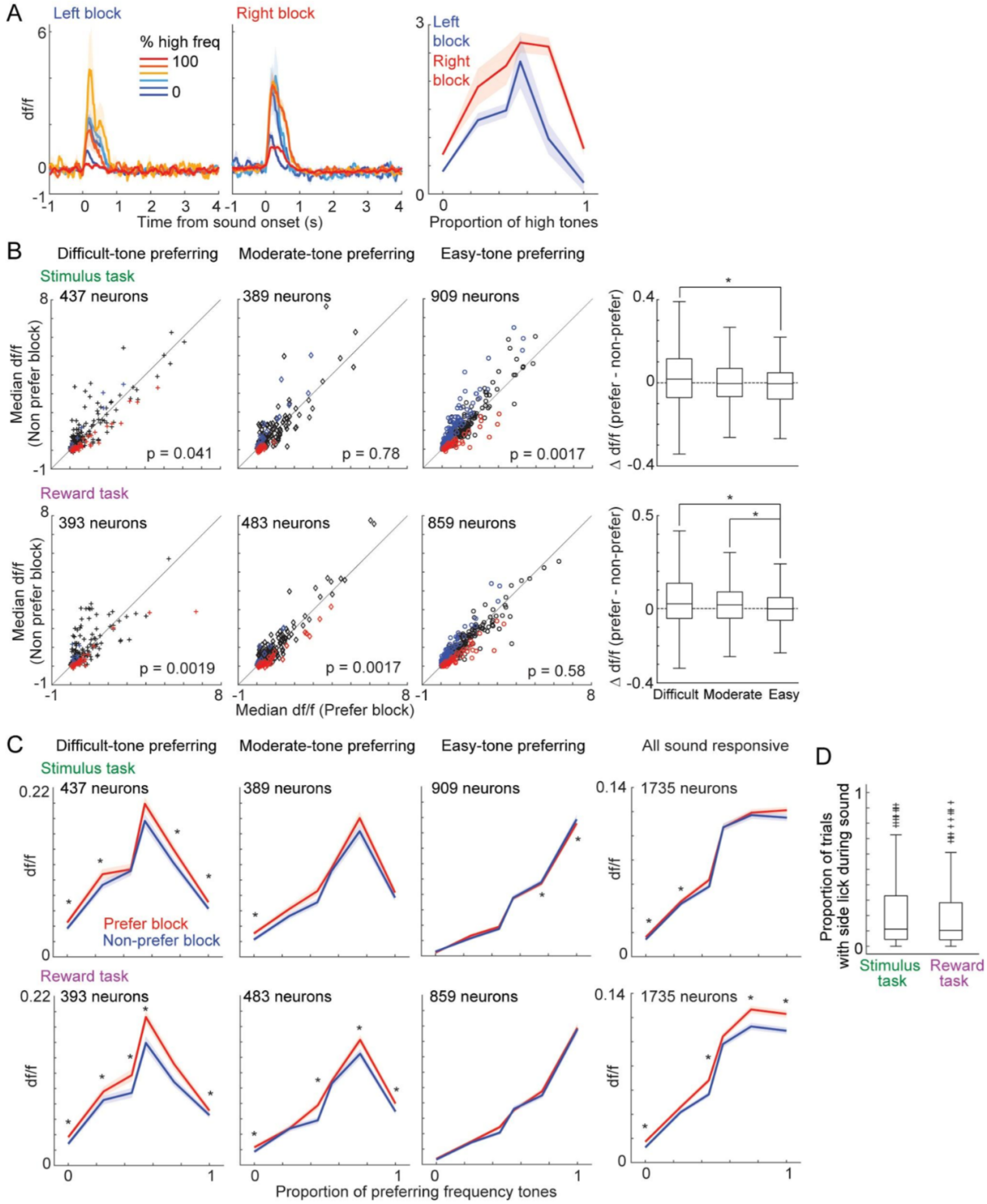

Supplemental Figure 6. Contextual modulation of activity in correct trials

(**A**) Traces of neuron in **Figure 3C** in correct trials. (**B, C**) Contextual modulation of sound responsive neurons in correct trials. Data presentations comply with **Figure 3 and S5**. (**B** *left* and **C**: two-sided Wilcoxon signed rank test, * $p < 0.01$; **B** *right*: *, $p < 0.01$ in two-sided Mann Whitney U-test). (**D**) Proportion of trials with side lick during sound (83 sessions in each task).

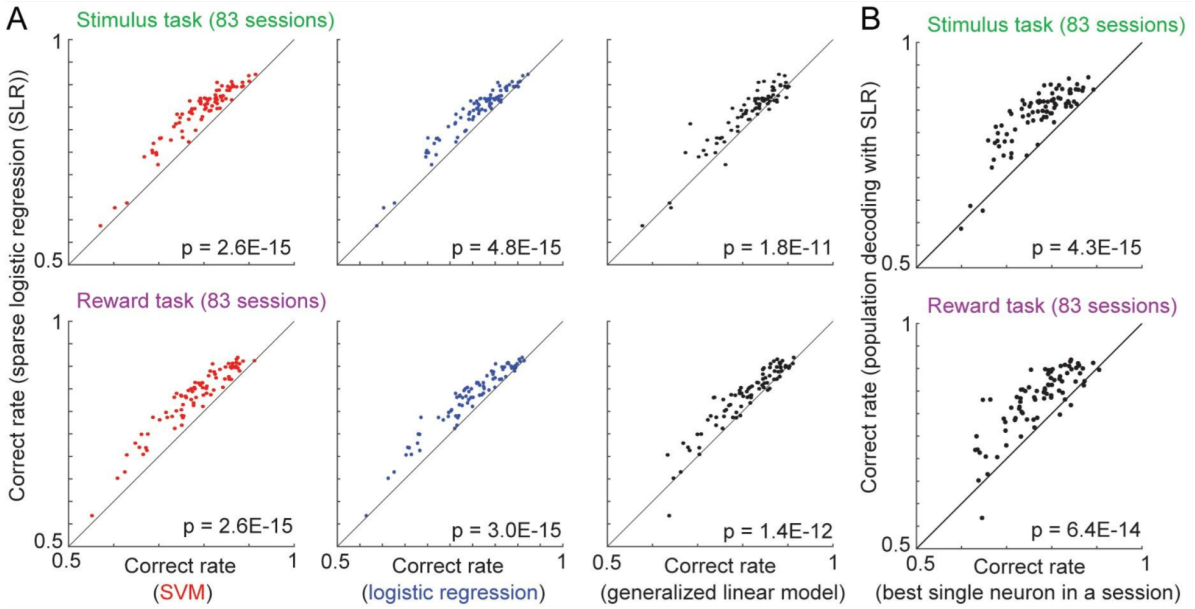

Supplemental Figure 7. Sound decoding with sparse logistic regression
(**A**) Sound decoding performance of sparse logistic regression (SLR) was compared with support vector machine (SVM), standard logistic regression, and generalized linear model (GLM). 10-fold cross validation was used (two-sided Wilcoxon signed rank test in 83 sessions). (**B**) Comparison of decoding performance between population (SLR) and single neuron in each session (two-sided Wilcoxon signed rank test in 83 sessions).

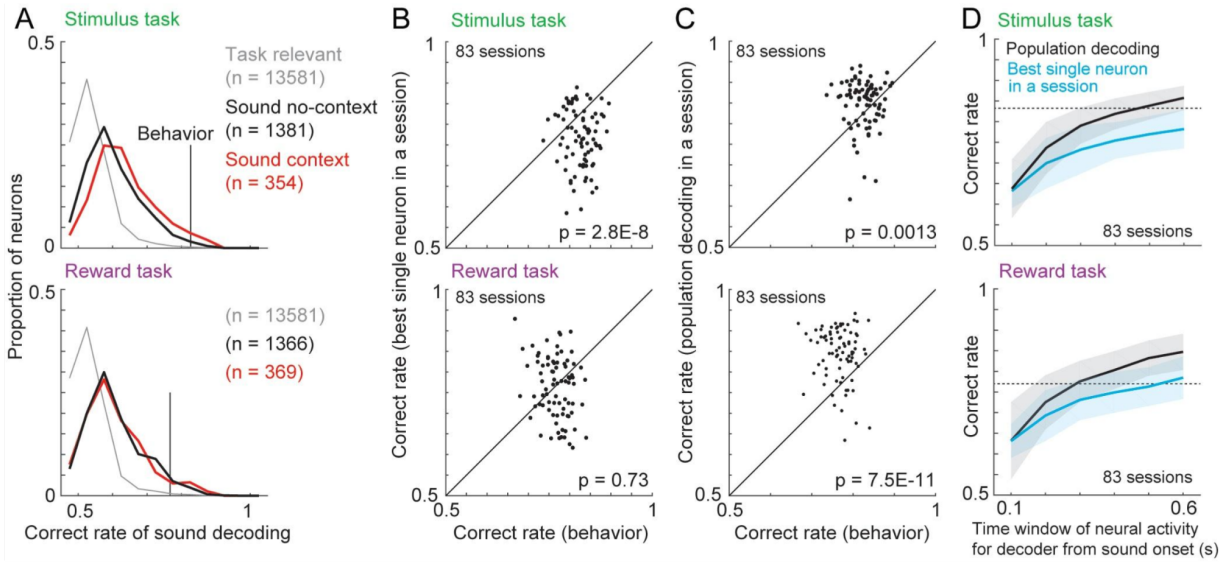

Supplemental Figure 8. Sound decoding with various time windows

(**A-C**) Decoders used the activity during 0.1 s at sound end. Data presentations comply with **Figure 4**. Although decoding only the final 0.1 seconds of sound yielded performance comparable to decoding the entire period (**Figure 4**), the results were confounded by the long time constant of the calcium signal, which effectively acted as an integrator. (**D**) Sound decoding performance with different length of time windows. Dot line shows the median performance of mouse behavior. The population sound decoding required the time window length of 500 ms and 300 ms in the stimulus and reward tasks to exceed the behavior. Medians and median absolute deviations.

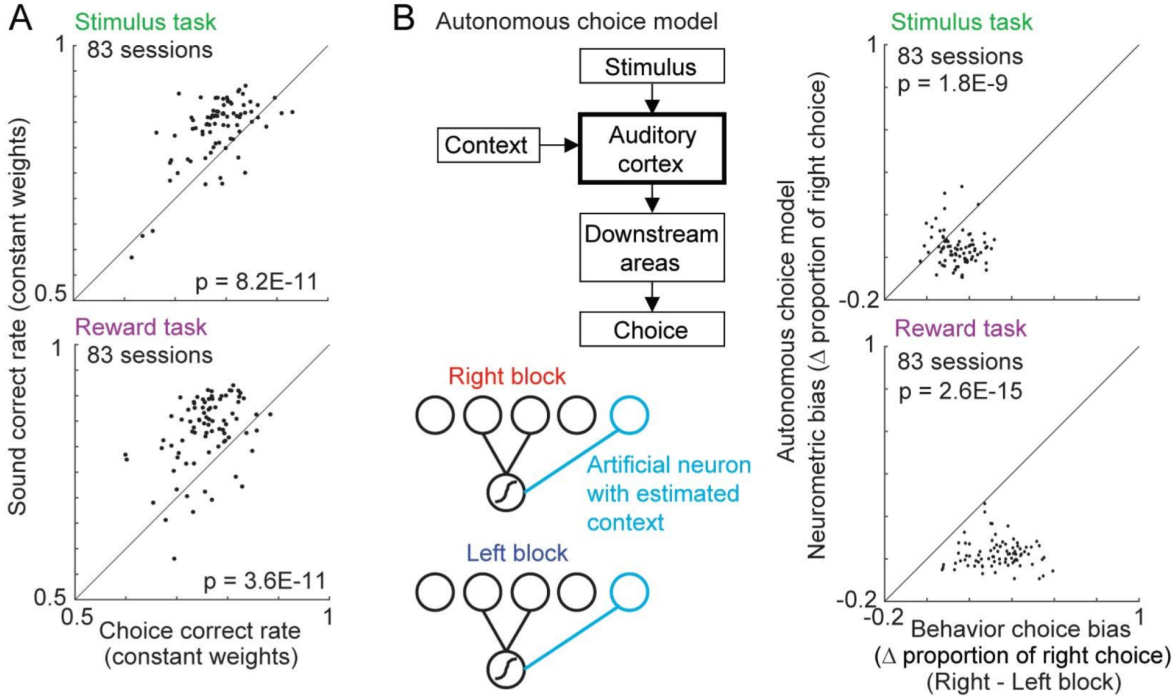

Supplemental Figure 9. Stable sound decoding from the auditory cortex
(**A**) Choice decoding with sparse logistic regression (SLR). Correct rate of sound decoding was higher than choice decoding during sound (two-sided Wilcoxon signed rank test in 83 sessions). (**B**) Autonomous choice model. Context was estimated from the activity of auditory cortex (*cyan neuron*) (**Figure 6G**) and used for the decoder. Data presentations comply with **Figure 6**.

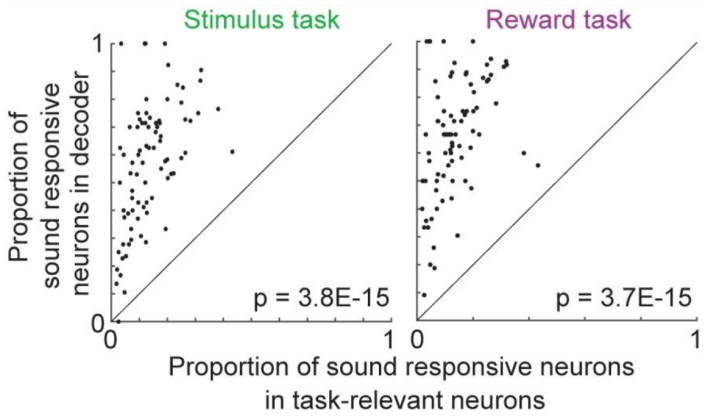

Supplemental Figure 10. Proportion of sound responsive neurons extracted in sparse logistic regression
Proportion of sound responsive neurons was compared between the neurons extracted in the decoder and that in task-relevant neurons (two-sided Wilcoxon signed rank test in 83 sessions).

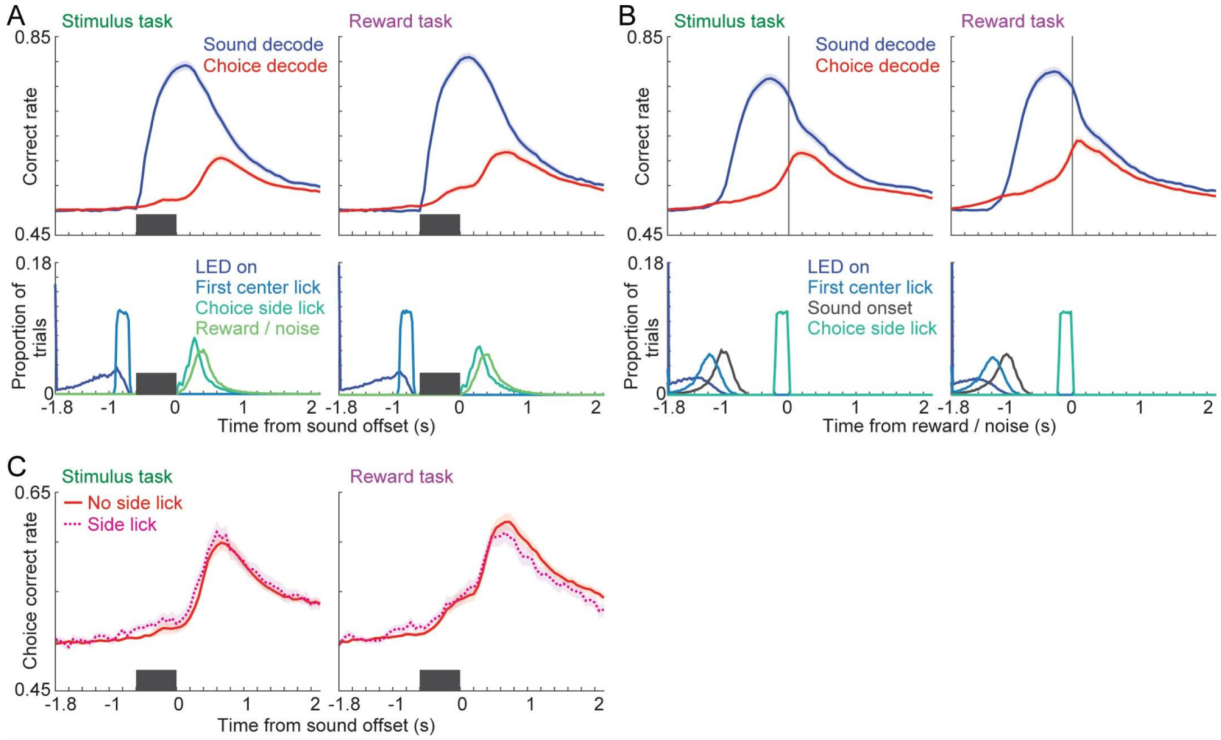

Supplemental Figure 11. Time course of sound and choice decoding

(**A, B**) Means and standard errors of decoding performance are shown in different timings (83 sessions in each task). Bottom panels show the timing of task variables. The decoding performance was aligned at the sound offset (**A**) and the reward / noise delivery (**B**). (**C**) Choice decoding without early side licks. Correct rate of choice decoding in each session was separately analyzed for the trials with early side licks and no-side licks during sounds. Means and standard errors (83 sessions in each task).

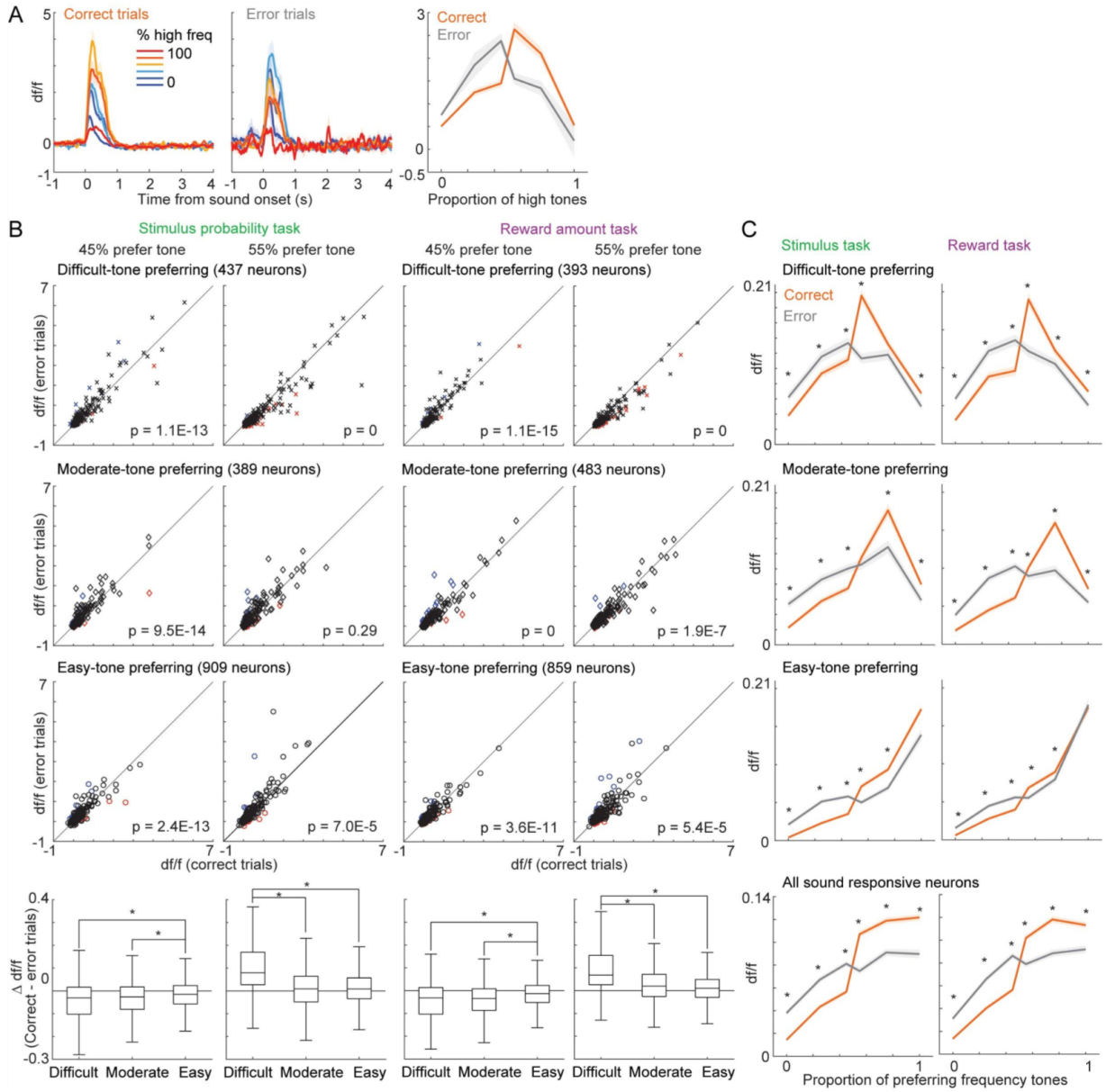

Supplemental Figure 12. Choice modulation of sound responsive neurons

(**A**) Choice modulation of neuron in **Figure 3C**. Data presentations comply with **Figure 3** but for correct and error trials. (**B**) Choice modulations of sound responses. Data presentations comply with **Figure 3 and S6**. Median activity of each neuron during 55 % and 45 % preferring tone cloud were compared between correct and error trials (*top*, two-sided Wilcoxon signed rank test). Large choice modulation in the difficult-tone preferring neurons (*bottom*, *, $p < 0.01$ in two-sided Mann Whitney U-test). Box plots without outliers. (**C**) Summary of choice modulation. Medians and robust standard errors (*, $p < 0.01$ in two-sided Wilcoxon signed rank test).

Methods

All animal procedures were approved by the Cold Spring Harbor Laboratory Animal Care and Use Committee in an Association for Assessment and Accreditation of Laboratory Animal Care (AAALAC International)-accredited facility and carried out in accordance with National Institutes of Health standards. Mice were housed in a temperature-controlled room with non-inverted, normal 12h/12h light/dark cycle.

Chronic window preparation

We used 6 male transgenic GCaMP6f mice (ai93+/–; lsl-tTA+/+; emx-cre+/–) (ai93, Jax stock 024103; lsl-tTA, Jax stock 008600; emx-cre, Jax stock 005628), 8 to 20 weeks of age (Gorski et al. 2002; Madisen et al. 2015; Musall et al. 2019; Wang et al. 2008). Before surgery, mice were restricted to 1.5 mL of water per day for at least two weeks. Mouse weight was checked daily to avoid dehydration. Two days before surgery, mice got free water access. The surgery had two steps. On day 1, we implanted a head bar for head-fixation of mice. On day 2, after recovery from the head-bar surgery, we implanted the cranial window over the auditory cortex.

For the head-bar surgery (day 1), mice were implanted with a custom designed light-weight head bar. Mice were anesthetized with isoflurane (1.5% at induction, below 1% to maintain) with an additional analgesic (meloxicam 2mg/kg, subcutaneous) and eye ointment. The mice were placed in a stereotaxic apparatus. The scalp was removed above the entire cortical area. The skull was cleaned with hydrogen peroxide. The head bar was attached to the skull with metabond adhesive (parkell, S380). The craniotomy surgery (day 2) was done under isoflurane anesthesia, using the headbar to immobilize the head. Eye ointment was applied. Meloxicam (2 mg/kg, subcutaneous), enrofloxacin (5mg/kg subcutaneous) and dexamethasone (2 mg/kg subcutaneous) were administered (Holtmaat et al. 2009). Enrofloxacin was also applied once per week to further prevent infection after surgery. After opening the skin, lidocaine was injected to the muscle above the auditory cortex. The muscle was removed and a craniotomy was made over the left hemisphere of auditory cortex (2.9 mm posterior and 4.2 mm lateral of the bregma) with a diameter of 3 mm, without puncturing the dura mater. A 3 mm diameter glass window (CS-3R, Warner Instruments) was mounted directly onto the dura and sealed with a mixture of krazy glue and dental acrylic powder (Lang, Jet denture repair powder/liquid). After surgery, water was given freely until the mouse recovered.

After recovery from surgery, behavioral training started. Mouse weight was carefully monitored, and additional water was given after daily training to keep the weight over 85% of the pre-restriction weight.

Behavioral training

Behavioral setup. The setup including part numbers and 3D print files was described before (Marbach and Zador 2016). The setup was placed inside a custom sound booth by Industrial Acoustics Company (Bronx, New York). The training was done with head-restrained mice positioned over a cylindrical treadmill running on ball bearings. The rotation of the treadmill was measured with a rotary encoder (200 P/R, Yumo). Two speakers (Avisoft Bioacoustics) were placed diagonally in front of mice for auditory stimulation. The speakers were calibrated with a

free-field microphone (Type 4939, Brüel and Kjaer) (Jaramillo and Zador 2014). Water was delivered through 19 gauge stainless steel tubing connected to solenoid valves (Lee Company) located outside the sound box. Water was calibrated weekly and was delivered through three spouts connected to a custom lick detection circuit. The behavioral system was controlled by a custom Matlab (Mathworks) program running on Bpod framework (https://sanworks.io) in Linux.

Task structure. The tone frequency discrimination task required mice to select the left or right spout depending on the frequency of the sound stimulus. Mice were required to withhold licking for 0.5 sec before a trial start. A blue LED indicated the trial start (end of inter-trial-interval) and mice were required to lick the center spout to start a sound stimulus with a delay of 0.1 to 0.3 sec. The sound stimulus was a 'tone cloud' stimulus as described before (Znamenskiy and Zador 2013) (see below). At the end of the tone cloud, mice received a small reward of water (0.5 μl) at the center spout. During the sound stimulus, mice were allowed to lick any spout. When the tone cloud contained more low tones than high tones (low category tone), the selection of left or right spout provided a large reward (2 μl of 2% sucrose water) (correct) or a noise burst (0.2 sec) (error), respectively. The high category tone cloud had the opposite correct and error choices. The time between the side lick and reward/noise varied between 0 and 0.2 sec. The interval of tone cloud between trials was at least 5.4 sec (6.6 sec in median), except in 1 out of 96,420 trials in 166 sessions (4.4 sec), to eliminate a sound adaptation in the auditory cortex. When mice did not select the side spout within 30 sec from the trial start, a new trial started.

Stimulus generation. The tone cloud was 0.6 sec long and consisted of a series of 30 ms pure tones with rise/decay ramps of 3 ms, presented at a rate of 100 tones per second. The frequency of each tone was sampled from the bottom 6 and top 6 tones of 18 logarithmically spaced slots (5 to 40 kHz). The tone cloud in each trial contained the low (5 – 10 kHz) or high frequency tones (20 – 40 kHz), and was categorized as low or high depending on the dominant frequency. The proportion of high tones in each tone cloud was selected from 6 settings (0, 0.25, 0.45, 0.55, 0.75, 1) with the probability of (25%, 12.5%, 12.5%, 12.5%, 12.5%, 25%, i.e., 2:1:1:1:1:2). In the stimulus probability task, we changed the probability between categories (see below) but kept the stimulus probability within the category constant (i.e., 2:1:1). The intensity of tone cloud was constant in each trial, but sampled from either 70, 75 or 80 dB SPL (sound pressure level in decibels with respect to 20 μPa) to discourage mice from using loudness to solve the task.

Stimulus probability and reward amount tasks. Every session started with an easy block where only the 100% low or high tone clouds were presented 60 to 80 trials with the stimulus probability of 50%-50% (low-high). The stimulus probability task then changed the stimulus probability of the low or high category tones in blocks of 175 to 220 trials (200 trials in 70 out of 83 sessions). The stimulus probability of one block started with either 70%-30% (low-high, left block) or 30%-70% (right block), and the probability reversed in the next block. After mice

experienced the two blocks, the stimulus probability became 50%-50% for the rest of the session. The reward amount for the correct choice was constant in all trials (2 μl).

The reward amount task changed the reward amount of the left and right spout in blocks, while the stimulus probability was 50%-50% (low-high) in all trials. In each block, the reward amount for the left-right correct choice was either 3μl-1μl or 1μl-3μl (left or right block). The block schedule was the same as in the stimulus probability task.

Training schedule. The initial phase of training was described previously (Marbach and Zador 2016). On the first day of training, we used only stimuli with 0.1 or 0.9 proportion high tones and free sucrose water from the correct side spout (free-reward trials). From the second day of training, we mixed the free-reward trials and the choice trials which required mice to select side spouts to get reward. Mice learned to lick the side spouts independently, presumably by feeling the delivery of the free-reward and licking towards it. We gradually decreased the proportion of free-reward trials. Based on performance (no strict criteria), we introduced more difficult tone clouds. The inter-trial-interval was then increased gradually by 3 days of training. We introduced the stimulus probability task and reward amount task after mice succeeded in getting reward in the task without any manipulations of stimulus or reward (about 90 % correct in 100 % low or high tone clouds).

Recording schedule. Each mouse performed both the stimulus probability task and reward amount task. We imaged the same field of view (FOV) and neurons during both tasks as follows: we imaged from one FOV during the stimulus probability task (day 1) and reward amount task (day 2), then switched to another FOV during reward amount task (day 3) and stimulus probability task (day 4). Day 5 had the same procedure as day 1 and so on. We did not use the following sessions for analysis: (i) mice did not complete the two blocks with opposite stimulus probability or reward amount in a given session, (ii) mice made errors in more than 25 % of trials with either the 100 % low or high tone cloud. In these cases, the same combination of FOV and task was selected the next day. Exceptionally, the same FOV was imaged in 11 and 2 sessions in the stimulus probability and reward amount tasks, respectively. In these sessions, we selected one session for analysis only based on the behavior data without analyzing the imaging data. Also, sessions described below were not used in the analyses: (i) the FOV was imaged only during either stimulus probability or reward amount task (7 and 1 sessions in stimulus and reward task), (ii) the FOV had a few bright cells which might indicate over-expressed GCaMP6f (1 session each task), (iii) the difference of imaging date between the two tasks was 17 days (1 session). In total, we analyzed 83 sessions in both the stimulus probability and reward amount task. The difference of imaging date between tasks was typically one day (1 day difference, 60 session pairs; 2 days, 15 pairs; 3 days, 7 pairs; 4 days, 1 pair).

Wide-field imaging

To identify the position of primary auditory cortex and determine the locations for two-photon imaging, we conducted one-photon wide-field calcium imaging through the chronic window.

Mice were awake and head-fixed on the treadmill. Two blue LEDs were used for illumination through fiber guides directed on the window. Emitted photons were captured by a CCD camera (Vosskuehler 1300QF). Frames were acquired at 4 Hz using a custom Labview software (National Instruments). Sound stimuli were presented at approximately every 6 s. Each stimulus was a 2 s train of pure tone pulses (20 Hz) at the frequency of either 4, 11 or 32 kHz with the intensity of 70 dB SPL. The sound evoked activity (F) was analyzed in each pixel as follow:

$$\frac{dF}{F} = (s - b)/b, \quad (1)$$

where s and b were the average intensity of stimulus (2 s, 8 frames) and pre-stimulus frames (2 s, 8 frames), respectively. Each frequency tone was repeated 10 times in a pseudo random order (30 stimuli in total). The location of primary auditory cortex was estimated to be the posterior-most spot of activity evoked by the 4 kHz tone (**Figure 2**).

Two-photon imaging

After training in the task, we started imaging experiments. As we observed almost no clearly over-expressing cells with GCaMP6f in our transgenic mice, we continued the experiments for 4 to 12 weeks. We imaged 9 to 21 fields of view (FOVs) from 2 to 3 selected XY locations per mouse (**Figure 2 and S2**). The depths of FOVs were between 110 and 510 μm. The FOVs were mainly from layers 2 and 3 (79 out of 83 sessions below 400 μm). On each experimental day, we imaged one FOV of one location.

Imaging was performed using a custom-built two-photon microscope with the objective lens at an adjustable angle to image auditory cortex without tilting the mouse. The resonant scanner was outside of the sound box, rendering it inaudible inside the box. We used a 20x/N.A. 1.0 water immersion objective for imaging (Olympus). A Ti:sapphire laser (Chameleon, Coherent) was operated at 910 nm to excite fluorescence, which was detected with GaAsP photomultiplier tube (Hamamatsu) in the spectral range of 500 – 540 nm (Chroma ET520/40m-2p). A 12kHz resonant scanning system was used to acquire images at 45 Hz at a resolution of 512 x 512 pixels corresponding to a 380 x 550 μm^2 field of view with the 20x objective. The microscope and image acquisition were controlled by an open source software (ScanImage, Vidrio Technologies, (Pologruto et al. 2003)). In each task session, we imaged for about one hour continuously in more than 500 trials. When slow drift of the imaging plane was observed, the objective position was manually adjusted (typically 1 μm at a time) during the inter-trial interval to match the recording site as precisely as possible to an average image taken at the beginning of the session.

Data analysis

All analyses were conducted with Matlab (MathWorks). In the figures, error bars of the mean represent standard deviation or standard error of the mean (s.e.m.). Error bars of the median represent median absolute deviation (MAD) or robust standard error (1.4826*MAD/sqrt(n); n = number of data points) (Adesnik et al. 2012).

Behavioral analysis. In every behavioral task session (one per day, one imaging plane at one location), trials in which mice succeeded to select the left or right spout were analyzed. In total, we analyzed 166 sessions from 6 mice from the stimulus probability task (83 sessions) and reward amount task (83 sessions) (mouse1, 20 sessions; mouse2, 42 sessions; mouse3, 28 sessions; mouse4, 24 sessions; mouse5, 34 sessions; mouse6, 18 sessions). Each field of view (FOV) was imaged during the two tasks.

We used a logistic regression to quantify the behavior bias between blocks (psychometric function) (**Figure 1**). The same equation was used to analyze the neurometric function of single and population neurons described later (**Figure 4 and 6**) (Klein 2001):

$$p = \lambda_1 + \frac{1-\lambda_1-\lambda_2}{1+exp(-A)},$$

$$A = \beta_0 + \beta_1 E_{high} + \beta_2 S + \beta_3 S \times E_{high}, \qquad (2)$$

where p was the probability to select the right spout. β_{0-3} were regression coefficients. β_1 determined the slope of the psychometric curve of behavior (stimulus sensitivity). β_2 quantified the choice bias between the left and right blocks, while β_3 quantified the change of stimulus sensitivity by blocks. λ_1 and λ_2 were lapse rates which were $\lambda_1 = \lambda_2$ for the model fitting in **Figure 1E**. E_{high} was the proportion of high frequency tones in a tone cloud. E_{high} had 6 settings (0, 0.25, 0.45, 0.55, 0.75 1). S was -1 or 1 for the left or right block. For model fitting, we used the trials only during left and right blocks.

To determine which parameters were relevant for mice behavior, we used a likelihood ratio test for the averaged log likelihood across sessions (**Figure 1E**) (Daw 2011). The parameters were set to achieve the maximum likelihood. In addition, we modeled the mice behavior in each block with the full-parameter logistic regression model (equation 2). This full model was used to analyze the difference of right choice probability between blocks (Δ fraction rightward) based on the average choice probability in logistic regression in each block (**Figure 1D and 6**). As the full model was independently applied to the data in each block, β_2 and β_3 were set to 0 (4 parameters in total).

Neural analysis. We used an open source software, Suite2P, for the motion correction and extraction of regions of interest (ROIs) from raw imaging data (https://github.com/cortex-lab/Suite2P) (Pachitariu et al. 2007). The parameters for Suite2P were default except the diameter of ROIs as 15. ROIs were then manually extracted with the GUI in Suite2P. Suite2P also detected the overlapping ROIs between the images taken during the stimulus probability task and reward amount task. The parameters for overlap detection were default (proportion of overlap, 0.6). In each ROI, a neuropil correction was done based on Suite2P. $\frac{dF}{F}(t)$ was calculated based on the signal at frame t, $F(t)$, as follows:

$$\frac{dF}{F}(t) = \frac{F(t)-F_0}{F_0}, \quad (3)$$

where F_0 was the average signal during 1 sec (45 frames) before the LED onset (trial start) in each trial.

Task-relevant neurons. For every ROI, $\frac{dF}{F}(t)$ were analyzed at the following 6 time windows during the task to investigate task-relevant neurons: (i) between the LED and sound onsets; (ii) during the sound presentation (0.6 sec); (iii) between 0 and 1 sec from the choice; (iv) between 1 and 2 sec from the choice; (v) between 0 and 1 sec from the reward or noise-burst delivery; (vi) between 1 and 2 sec from the reward or noise-burst delivery. The neural activity was analyzed in the following trials in each time window: (i, ii) all, low-, or high-category-tone trials; (iii, iv) all, left-, or right-choice trials; (v, vi) all, reward, or noise-burst trials (3 conditions in each time window). This analysis was independently applied to the activity during the stimulus probability task and reward amount task. We defined the ROI as task-relevant when the aligned and averaged activity had a significantly positive value at any time window (6 settings), in any condition (3 settings), and in any task (2 settings) compared to the baseline activity (36 settings in total (6 x 3 x 2)) (one-way Wilcoxon signed rank test $p < 0.001$ in each comparison). The baseline activity was defined as the activity before the LED onset with the corresponding time window in each condition. The activity during left and right blocks was used in the analyses here and hereafter.

Neural encoding. We investigated the activity of sound responsive neurons which had (1) significant increase of activity during sounds (time window of (ii) in previous section) and (2) preferred tone cloud ($p < 0.01$ in Kruskal-Wallis test) in both the stimulus probability and reward amount tasks. The preferred tone cloud of each neuron was defined as the stimulus with the highest average activity in correct trials. The activity of sound responsive neurons were compared between left and right blocks to identify the block (context) modulated neurons which had significant change of activity between blocks at the preferred tone cloud ($p < 0.05$, two-sided Mann Whitney U-test) (**Figure 3**). The activity was also compared between correct and error trials (**Figure S11**).

Signal and noise correlation. Signal and noise correlations were investigated using the Pearson correlation coefficient between pairs of sound-responsive neurons. Signal correlation was defined as the correlation coefficient between the mean activity of each 6 tone cloud in a given neuron pair (Miura et al. 2012). For the noise correlation, the calcium traces for each of 6 tone clouds were independently z-scored (mean subtracted and divided by the standard deviation) to get the variability of activity in each stimulus. The noise correlation was defined as the correlation coefficient between the variability (noise) of neuron pairs.

Single neuron decoding. Our decoder for single neurons used a simple threshold to categorize the neural activity into low and high tones (**Figure 4**). The average activity during sound was used in the decoder. The threshold was computed from the training data in 10-fold cross validation and

tested in the validation data. The cross validation was applied 100 times to reduce the variance of decoding performance from the random grouping. As the 10-fold cross validation analysis estimated 10 different thresholds for one neuron (or 1000 thresholds in our analysis), we also investigated one optimal threshold using all the data from one single neuron to investigate the relationship between the decoding threshold, decoding performance, and block-dependent modulation (**Figure 7**). The block modulation was defined as the difference of median activity between blocks at the preferred tone cloud. The decoding threshold and block modulation were z-scored (mean subtracted and divided by the standard deviation) for population analysis.

Population neural decoding. We used a sparse logistic regression (SLR) to decode sound category (low or high) from the population activity of task-relevant neurons. We used a software package, sparse learning package (SLEP) (https://github.com/jiayuzhou) (Liu et al. 2009). First, a logistic regression provided the likelihood of decoding performance as follows:

$$p(S|F,\beta) = \frac{1}{1+exp(\beta_0+\sum_{i=1}^{N}\beta_i F_i)}, \quad (4)$$

where S was the tone category. F_i was the average activity ($\frac{dF}{F}(t)$) of each neuron during sounds. N was the number of task-relevant neurons in each session. β_i was the coefficient for neuron i. The SLR minimized the following equation with the regularization parameter λ:

$$-\frac{1}{T}\sum_{trial=1}^{T} log(p(S|F,\beta)) + \lambda\sum_{i=1}^{N}\left|\beta_i\right|. \quad (5)$$

We used nested 10-fold cross validation to evaluate the decoding performance (Shimizu et al. 2015). First, trials of left and right blocks in one session were equally divided into 10 groups. The 9 groups of data were used to train the SLR, while the remaining 1 group was used to validate the decoding performance. We repeated all the 10 combinations of training and test data to evaluate the performance in all trials. The regularization parameter λ was determined with a 10-fold cross validation within the training data (9 groups of original data), such that the test data (the remaining 1 group of data) was neither used to determine λ nor β. The nested cross validation was applied 100 times to reduce the variance of decoding performance from the random grouping. The likelihood of SLR was binarized at 0.5 (decision threshold) to get the correct rate in each session. The non-autonomous choice model had the optimal block-dependent decision thresholds (**Figure 6E**). The neurometric function in each block was analyzed based on the binarized likelihood in SLR. Δ choice bias in the neurometric function was analyzed with the full-parameter logistic regression model which was independently applied in each block (equation 2) (**Figure 4 and 6**).

We investigated the sound decoding performance on shuffled neural data to assess the effect of noise correlations on population neural decoding (Figure 5D). In every task-relevant neuron, we swapped the activity for 2 trials with the same tone cloud and investigated whether the swap increased or decreased the correlations among neurons. If the average population correlations decreased with the swap, we accepted the swap and otherwise rejected. In each neuron in each

tone cloud, we repeated the swap 100 times. This shuffling changed the noise correlation among neurons but did not change the signal correlation and mean tone-evoked activity (Miura et al. 2012).

To compare the decoding performance of constant weights, dynamic weights, and discordant weights (**Figure 6A**), we trained the SLR by using an equal number of low- and high-category-tone trials in each block by subsampling the training data. This prevented the decoder from using the knowledge of stimulus probability for classification especially in the stimulus probability task. For training the SLR with dynamic weights, which had independent β and λ in each block, the nested cross validation was separately applied to the trials in left and right blocks. For training the SLR with constant weights, the nested 10-fold cross validation was applied once in the two blocks. The number of trials for training was adjusted such that the equal number of trials were used to train the SLR with dynamic and constant weights. Training of SLR with discordant weights was performed in the same way as the dynamic weights, but trained and tested with the different blocks.

The performance of SLR in sound decoding was compared with that of support vector machine (SVM) (MATLAB, fitcsvm), standard logistic regression (SLEP with λ close to 0), and generalized linear model (GLM) during sound (**Figure S7A**). The decoders had constant weights and used the activity of task-relevant neurons. For GLM, we used a log-linear model in which the log scale of neural activity was fit to a linear regression with task parameters (sound category, choice, block, outcome, licking frequency for three spouts (left, center, right), and locomotion speed). The relevant parameters were investigated with Lasso (software package, SLEP) with the nested 10-fold cross validation. GLM decoder then used Bayes' theorem to decode sound category from the log-linear model, assuming that the activity of each neuron was independent (Runyan et al. 2017).

Sound and choice decoding during the entire task. We investigated the decoding performance of sound and choice in 60 different time windows on trials that were selected to decorrelate the two variables (**Figure 8**). Each time window has 0.27 sec (12 frames) with a time step of 0.067 sec (3 frames). To decode sound category without the choice effect, we sub-selected either left- or right-choice trials and independently decoded the sound category. To decode choice without the sound effect, we sub-selected trials with each of 6 tone clouds and decoded the choice. The decoding performance was defined as the average of the 2 and 6 cases in the sound and choice decoding, respectively. All the decoding was done with nested 10-fold cross validation in SLR. The training data was sub-sampled such that the number of trials for each category was equal. The 10-fold cross validation was applied twice in this time-window analysis. The number of training data was different between the sound and choice decoding, making it difficult to directly compare the performance of the two decoders.

Pure tone response

After each two-photon imaging session during the task, we investigated the pure tone responsiveness of neurons. We presented pure tones (5 to 40 kHz with 18 logarithmically spaced slots, 30 ms with 3 ms rise/decay ramps, 50 or 75 dB SPL), white noise (30 ms with 3 ms rise/decay ramps, 50 or 75 dB SPL) and the tone clouds used during the task. The tone clouds were selected to contain 10 stimuli from each of 6 tone-cloud settings. We presented each stimulus in pseudo-random order with the inter-stimulus interval of 2 s. In total, we presented 440 stimuli (360 pure tones (18 frequencies x 2 intensities x 10 times); 20 white noise (2 intensities x 10 times); 60 tone clouds (6 settings x 10 times)).

Pure tones with 75 dB SPL were used to analyze the tone evoked responses of auditory cortical neurons. Based on the fluorescence intensity $F(t)$, $\frac{dF}{F}(t)$ in each ROI was calculated by the same procedure as for the task (equation 3), except that F_0 was the average fluorescence intensity during 1 s (45 frames) before the sound onset in each trial. Neural activity following the tone presentation of 2 adjacent frequencies was analyzed together (9 frequency categories). When the activity within 1 s from the tone onset was higher than the activity before sound at least in one of the 9 frequencies, we defined the neuron as tone responsive (one-sided Wilcoxon signed rank test, $p < 0.005$). The best frequency (BF) of the neuron was defined as the tone frequency which evoked the highest activity.

Based on the BFs, we investigated the tonotopic map in the auditory cortex. In each mouse, the imaging planes of all depths were superimposed to average the BFs in XY locations (each location 200 x 200 μm with 100 μm step) (**Figure 2 and S2**).

Statistics

All the statistical tests in this study were non parametric. We mainly used two-sided statistical tests. Clear statement was added where we used a one-sided test. In tests with multiple comparisons, we set the significance threshold according to the Bonferroni correction. Data collection and analyses were not performed blind to the conditions of the experiments. No statistical methods were used to pre-determine sample sizes but our sample sizes are similar to those generally used in the field.

Data and code availability

Data analyses were conducted in Matlab scripts which are available from the corresponding author upon request. The data that support the findings of this study are available from the corresponding author upon request.

References

Abbott, L. F., and Peter Dayan. 1999. "The Effect of Correlated Variability on the Accuracy of a Population Code." *Neural Computation* 11 (1): 91–101. https://doi.org/10.1162/089976699300016827.

Adesnik, Hillel, William Bruns, Hiroki Taniguchi, Z. Josh Huang, and Massimo Scanziani. 2012. "A Neural Circuit for Spatial Summation in Visual Cortex." *Nature* 490 (7419): 226–31.

Averbeck, Bruno B., Peter E. Latham, and Alexandre Pouget. 2006. "Neural Correlations, Population Coding and Computation." *Nature Reviews Neuroscience* 7 (5): 358–66. https://doi.org/10.1038/nrn1888.

Bialek, William, Fred Rieke, Rob R. De Ruyter Van Steveninck, and David Warland. 1991. "Reading a Neural Code." *Science* 252 (5014): 1854–7. https://doi.org/10.1126/science.2063199.

Bialek, William, Rob de Ruyter van Steveninck, Rieke Fred, and Warland David. 1996. *Spikes: Exploring the Neural Code*. The MIT Press.

Britten, K. H., M. N. Shadlen, W. T. Newsome, and J. A. Movshon. 1992. "The Analysis of Visual Motion: A Comparison of Neuronal and Psychophysical Performance." *Journal of Neuroscience* 12 (12): 4745–65.

Daw, Nathaniel D. 2011. "Trial-by-Trial Data Analysis Using Computational Models." *Decision Making, Affect, and Learning: Attention and Performance XXIII* 23: 3–38.

Driscoll, Laura N., Noah L. Pettit, Matthias Minderer, Selmaan N. Chettih, and Christopher D. Harvey. 2017. "Dynamic Reorganization of Neuronal Activity Patterns in Parietal Cortex." *Cell* 170 (5): 986–99.e16.

Feng, Samuel, Philip Holmes, Alan Rorie, and William T. Newsome. 2009. "Can Monkeys Choose Optimally When Faced with Noisy Stimuli and Unequal Rewards?" *PLoS Computational Biology* 5 (2): e1000284. https://doi.org/10.1371/journal.pcbi.1000284.

Fritz, Jonathan, Shihab Shamma, Mounya Elhilali, and David Klein. 2003. "Rapid Task-Related Plasticity of Spectrotemporal Receptive Fields in Primary Auditory Cortex." *Nature Neuroscience* 6 (11): 1216–23.

Gorski, Jessica A., Tiffany Talley, Mengsheng Qiu, Luis Puelles, John L. R. Rubenstein, and Kevin R. Jones. 2002. "Cortical Excitatory Neurons and Glia, but Not GABAergic Neurons, Are Produced in the Emx1-Expressing Lineage." *Journal of Neuroscience* 22 (15): 6309–14.

Green, D. M., and Swets, J. A. 1966. "Signal Detection Theory and Psychophysics." *Wiley*.

Guo, Lan, Jardon T. Weems, William I. Walker, Anastasia Levichev, and Santiago Jaramillo. 2019. "Choice-Selective Neurons in the Auditory Cortex and in Its Striatal Target Encode Reward Expectation." *Journal of Neuroscience*. 39 (19): 3687–97. https://doi.org/10.1523/JNEUROSCI.2585-18.2019.

Hanks, Timothy D., Mark E. Mazurek, Roozbeh Kiani, Elisabeth Hopp, and Michael N. Shadlen. 2011. "Elapsed Decision Time Affects the Weighting of Prior Probability in a Perceptual Decision Task." *Journal of Neuroscience.* 31 (17): 6339–52.

Hattori, Ryoma, Bethanny Danskin, Zeljana Babic, Nicole Mlynaryk, and Takaki Komiyama. 2019. "Area-Specificity and Plasticity of History-Dependent Value Coding During Learning." *Cell* 177 (7): 1858–72. https://doi.org/10.1016/j.cell.2019.04.027.

Holtmaat, Anthony, Tobias Bonhoeffer, David K. Chow, Jyoti Chuckowree, Vincenzo De Paola, Sonja B. Hofer, Mark Hübener, et al. 2009. "Long-Term, High-Resolution Imaging in the Mouse Neocortex through a Chronic Cranial Window." *Nature Protocols* 4 (8): 1128–44.

Hromádka, Tomáš, Michael R. Deweese, Anthony M. Zador, and S. Figs. 2008. "Sparse Representation of Sounds in the Unanesthetized Auditory Cortex." *PLoS Biology* 6 (1): e16.

Hubel, David H., Calvin O. Henson, Allen Rupert, and Robert Galambos. 1959. "'Attention' Units in the Auditory Cortex." *Science*. 129 (3358): 1279–80. https://doi.org/10.1126/science.129.3358.1279.

Issa, John B., Benjamin D. Haeffele, Amit Agarwal, Dwight E. Bergles, Eric D. Young, and David T. Yue. 2014. "Multiscale Optical Ca2+Imaging of Tonal Organization in Mouse Auditory Cortex." *Neuron*. 83 (4): 944–59. https://doi.org/10.1016/j.neuron.2014.07.009.

Jaramillo, Santiago, Katharine Borges, and Anthony M. Zador. 2014. "Auditory Thalamus and Auditory Cortex Are Equally Modulated by Context during Flexible Categorization of Sounds Average Trials per Session" *Journal of Neuroscience* 34 (15): 5291–5301.

Jaramillo, Santiago, and Anthony M. Zador. 2014. "Mice and Rats Achieve Similar Levels of Performance in an Adaptive Decision-Making Task." *Frontiers in Systems Neuroscience* 8 (173). https://doi.org/10.3389/fnsys.2014.00173.

Klein, Stanley A. 2001. "Measuring, Estimating, and Understanding the Psychometric Function: A Commentary." *Perception and Psychophysics*. 63 (8): 1421–55. https://doi.org/10.3758/BF03194552.

Knutsen, Per Magne, and Ehud Ahissar. 2009. "Orthogonal Coding of Object Location." *Trends in Neurosciences* 32 (2): 101–9.

Kravitz, Alexxai V., Lynne D. Tye, and Anatol C. Kreitzer. 2012. "Distinct Roles for Direct and Indirect Pathway Striatal Neurons in Reinforcement." *Nature Neuroscience*. 15 (6): 816–818. https://doi.org/10.1038/nn.3100.

Lak, Armin, Michael Okun, Morgane M. Moss, Harsha Gurnani, Karolina Farrell, Miles J. Wells, Charu Bai Reddy, Adam Kepecs, Kenneth D. Harris, and Matteo Carandini. 2020. "Dopaminergic and Prefrontal Basis of Learning from Sensory Confidence and Reward Value." *Neuron* 105 (4): 700–711. https://doi.org/10.1016/j.neuron.2019.11.018.

Liu, Jun, Shuiwang Ji, and Jieping Ye. 2009. "Sparse Learning with Efficient Projections." *Arizona State University*.

Madisen, Linda, Aleena R. Garner, Daisuke Shimaoka, Amy S. Chuong, Nathan C. Klapoetke, Lu Li, Alexander van der Bourg, et al. 2015. "Transgenic Mice for Intersectional Targeting of Neural Sensors and Effectors with High Specificity and Performance." *Neuron* 85 (5): 942–58.

Fred Marbach, and Anthony M. Zador. 2016. "A Self-Initiated Two-Alternative Forced Choice Paradigm for Head-Fixed Mice." *bioRxiv*, https://doi.org/10.1101/073783.

Ma, Wei Ji, Jeffrey M. Beck, Peter E. Latham, and Alexandre Pouget. 2006. "Bayesian Inference with Probabilistic Population Codes." *Nature Neuroscience* 9 (11): 1432–8. https://doi.org/10.1038/nn1790.

Keiji Miura, Zachary F. Mainen, and Naoshige Uchida. 2012. "Odor Representations in Olfactory Cortex: Distributed Rate Coding and Decorrelated Population Activity." *Neuron* 74 (6): 1087–98. https://doi.org/10.1016/j.neuron.2012.04.021.

Moreno-Bote, Rubén, Jeffrey Beck, Ingmar Kanitscheider, Xaq Pitkow, Peter Latham, and Alexandre Pouget. 2014. "Information-Limiting Correlations." *Nature Neuroscience* 17 (10): 1410–7. https://doi.org/10.1038/nn.3807.

Musall, Simon, Matthew T. Kaufman, Ashley L. Juavinett, Steven Gluf, and Anne K. Churchland. 2019. "Single-Trial Neural Dynamics Are Dominated by Richly Varied Movements." *Nature Neuroscience* 22 (10): 1677–86.

Otazu, Gonzalo H., Lung-Hao Tai, Yang Yang, and Anthony M. Zador. 2009. "Engaging in an Auditory Task Suppresses Responses in Auditory Cortex." *Nature Neuroscience* 12 (5): 646–54.

Pachitariu, Marius, Carsen Stringer, Sylvia Schröder, Mario Dipoppa, L. Federico Rossi, Matteo Carandini, Kenneth D. Harris, et al. 2007. "Suite2p: Beyond 10,000 Neurons with Standard Two-Photon Microscopy." *bioRxiv*, https://doi.org/10.1101/061507.

Pisupati, Sashank, Lital Chartarifsky-Lynn, Anup Khanal, and Anne K. Churchland. 2021. "Lapses in Perceptual Decisions Reflect Exploration." *eLife* 10: e55490.

Platt, M. L., and Paul W. Glimcher. 1999. "Neural Correlates of Decision Variables in Parietal Cortex." *Nature* 400 (6741): 233–38.

Pologruto, Thomas A., Bernardo L. Sabatini, and Karel Svoboda. 2003. "ScanImage: Flexible Software for Operating Laser Scanning Microscopes." *Biomedical Engineering Online* 2 (13). https://doi.org/10.1186/1475-925X-2-13.

Quirk, Gregory J., Jorge L. Armony, and Joseph E. LeDoux. 1997. "Fear Conditioning Enhances Different Temporal Components of Tone-Evoked Spike Trains in Auditory Cortex and Lateral Amygdala." *Neuron* 19 (3): 613–24.

Romero, Sandra, Ariel E. Hight, Clayton K. Kameron, Jennifer Resnik, Ross S. Williamson, Kenneth E. Hancock, and Polley B. Daniel. 2020. "Cellular and Widefield Imaging of Sound Frequency Organization in Primary and Higher-Order Fields of the Mouse Auditory

Cortex." *Cerebral Cortex*, 30 (3): 1603–22. https://doi.org/10.1093/cercor/bhz190.

Rumyantsev, Oleg I., Jérôme A. Lecoq, Oscar Hernandez, Yanping Zhang, Joan Savall, Radosław Chrapkiewicz, Jane Li, Hongkui Zeng, Surya Ganguli, and Mark J. Schnitzer. 2020. "Fundamental Bounds on the Fidelity of Sensory Cortical Coding." *Nature* 580 (7801): 100–105. https://doi.org/10.1038/s41586-020-2130-2.

Runyan, Caroline A., Eugenio Piasini, Stefano Panzeri, and Christopher D. Harvey. 2017. "Distinct Timescales of Population Coding across Cortex." *Nature* 548 (7665): 92–96.

Schneider, David M., Anders Nelson, and Richard Mooney. 2014. "A Synaptic and Circuit Basis for Corollary Discharge in the Auditory Cortex." *Nature* 513 (7517): 189-94. https://doi.org/10.1038/nature13724.

Shimizu, Yu, Junichiro Yoshimoto, Shigeru Toki, Masahiro Takamura, Shinpei Yoshimura, Yasumasa Okamoto, Shigeto Yamawaki, and Kenji Doya. 2015. "Toward Probabilistic Diagnosis and Understanding of Depression Based on Functional MRI Data Analysis with Logistic Group LASSO." *PloS One* 10 (5): e0123524. https://doi.org/10.1371/journal.pone.0123524.

The International Brain Laboratory, Valeria Aguillon-Rodriguez, Dora Angelaki, Hannah Bayer, Niccolo Bonacchi, Matteo Carandini, Fanny Cazettes, et al. 2021. "Standardized and Reproducible Measurement of Decision-Making in Mice." *eLife* 10: e63711. https://doi.org/10.7554/eLife.63711.

The International Brain Laboratory. 2017. "An International Laboratory for Systems and Computational Neuroscience." *Neuron* 96 (6): 1213–18. https://doi.org/10.1016/j.neuron.2017.12.013.

Ulanovsky, Nachum, Liora Las, and Israel Nelken. 2003. "Processing of Low-Probability Sounds by Cortical Neurons." *Nature Neuroscience* 6 (4): 391-8. https://doi.org/10.1038/nn1032.

Wang, Lijun, Kamal Sharma, Han-Xiang Deng, Teepu Siddique, Gabriella Grisotti, Erdong Liu, and Raymond P. Roos. 2008. "Restricted Expression of Mutant SOD1 in Spinal Motor Neurons and Interneurons Induces Motor Neuron Pathology." *Neurobiology of Disease* 29 (3): 400–408.

Znamenskiy, Petr, and Anthony M. Zador. 2013. "Corticostriatal Neurons in Auditory Cortex Drive Decisions during Auditory Discrimination." *Nature* 497 (7450): 482–85.

Zohary, E., M. N. Shadlen, and W. T. Newsome. 1994. "Correlated Neuronal Discharge Rate and Its Implications for Psychophysical Performance." *Nature* 370 (6485): 140–3.

Acknowledgements

We thank B. Burbach for technical assistance, J. Cohen and V.R. Aguillon for behavior training, H. Zeng for providing Ai93 mice. This work was supported by Uehara Memorial Foundation (A.F.), the Watson School of Biological Sciences Farish-Gehry Fellowship (F.M.) and the National Institutes of Health () (A.Z).

Author contributions

A.F., F.M. and A.M.Z. designed the experiments. F.M. built the setup for experiments. A.F. and F.M. performed the experiments. A.F. analyzed the data. A.F., A.Z. wrote the paper, with comments by F.M.

Competing interests

A.Z. is a founder of Cajal Neuroscience. F.M. and A.F. declare no competing financial interests.

Materials & Correspondence

Should be addressed to A.F.